

## Article

# Catalytic Upgrading of Plastic Waste of Electric and Electronic Equipment (WEEE) Pyrolysis Vapors over Si–Al Ash Pellets in a Two-Stage Reactor

Augusto Fernando de Freitas Costa <sup>1</sup>, Caio Campos Ferreira <sup>1</sup>, Simone Patrícia Aranha da Paz <sup>1</sup>, Marcelo Costa Santos <sup>1</sup> , Luiz Gabriel Santos Moreira <sup>2</sup>, Neyson Martins Mendonça <sup>2</sup>, Fernanda Paula da Costa Assunção <sup>3</sup>, Ana Carolina Gomes de Albuquerque de Freitas <sup>4</sup>, Roseane Maria Ribeiro Costa <sup>4</sup> , Isaque Wilkson de Sousa Brandão <sup>5</sup> , Carlos Emmerson Ferreira da Costa <sup>5</sup>, Sílvio Alex Pereira da Mota <sup>6</sup>, Douglas Alberto Rocha de Castro <sup>7</sup> , Sergio Duvoisin, Jr. <sup>8</sup>, Luiz Eduardo Pizarro Borges <sup>9</sup>, Nélvio Teixeira Machado <sup>1,2,\*</sup>  and Lucas Pinto Bernar <sup>1</sup>

<sup>1</sup> Graduate Program of Natural Resources Engineering of Amazon, Campus Profissional-UFPA, Universidade Federal do Pará, Rua Augusto Corrêa N° 1, Belém 66075-110, Brazil

<sup>2</sup> Faculty of Sanitary and Environmental Engineering, Campus Profissional-UFPA, Universidade Federal do Pará, Rua Corrêa N° 1, Belém 66075-900, Brazil

<sup>3</sup> Graduate Program of Civil Engineering, Campus Profissional-UFPA, Universidade Federal do Pará, Rua Augusto Corrêa N° 1, Belém 66075-110, Brazil

<sup>4</sup> Graduate Program of Pharmaceutical Sciences, Campus Profissional-UFPA, Universidade Federal do Pará, Rua Augusto Corrêa N° 1, Belém 66075-110, Brazil

<sup>5</sup> Graduate Program of Chemistry, Universidade Federal do Pará, Rua Augusto Corrêa N° 1, Belém 66075-110, Brazil

<sup>6</sup> Graduate Program of Chemistry, Universidade Federal do Sul e Sudeste do Pará, Folha 31, Quadra 7, Lote Especial—Nova Marabá, Marabá 68507-590, Brazil

<sup>7</sup> Centro Universitário Luterano de Manaus—CEULM/ULBRA, Avenida Carlos Drummond de Andrade N° 1460, Manaus 69077-730, Brazil

<sup>8</sup> Faculty of Chemical Engineering, Universidade do Estado do Amazonas-UEA, Avenida Darcy Vargas N° 1200, Manaus 69050-020, Brazil

<sup>9</sup> Laboratory of Catalyst Preparation and Catalytic Cracking, Section of Chemical Engineering, Instituto Militar de Engenharia-IME, Praça General Tibúrcio N° 80, Rio de Janeiro 22290-270, Brazil

\* Correspondence: machado@ufpa.br; Tel.: +55-91-984-620-325



**Citation:** de Freitas Costa, A.F.; Ferreira, C.C.; da Paz, S.P.A.; Santos, M.C.; Moreira, L.G.S.; Mendonça, N.M.; da Costa Assunção, F.P.; de Freitas, A.C.G.d.A.; Costa, R.M.R.; de Sousa Brandão, I.W.; et al.

Catalytic Upgrading of Plastic Waste of Electric and Electronic Equipment (WEEE) Pyrolysis Vapors over Si–Al Ash Pellets in a Two-Stage Reactor. *Energies* **2023**, *16*, 541. <https://doi.org/10.3390/en16010541>

Academic Editor: Diego Luna

Received: 29 November 2022

Revised: 27 December 2022

Accepted: 28 December 2022

Published: 3 January 2023



**Copyright:** © 2023 by the authors. Licensee MDPI, Basel, Switzerland. This article is an open access article distributed under the terms and conditions of the Creative Commons Attribution (CC BY) license (<https://creativecommons.org/licenses/by/4.0/>).

**Abstract:** This study investigated thermal cracking and catalytic upgrading of waste from electric and electronic equipment (WEEE) plastics on a semi-batch reactor coupled to a heated catalyst fixed bed (2-stage vapor cracking). The catalyst used is a Si–Al ash obtained from commercial activated carbon pellets treated with concentrated NaOH solution and calcination. The purpose of the study was to characterize the waste stream through its thermogravimetry analysis and pyrolysis products, study the effect of temperature (350–500 °C) and catalyst quantity (0.0–7.5 %wt) on yields of reaction products, physical chemical properties, and chemical composition of bio-oil in order to understand and evaluate production of fuels and chemical feedstock by recycling of WEEE plastic through catalytic upgrading. Time-fractioned samples were taken in determined reaction times (15, 30, 45, and 60 min) to study the evolution of cracking reactions during experiment runs through changes to chemical composition (GC/MS). A comparison with other previous work is also presented to show similarities between different feedstocks using the same thermal unit. The results indicate composition of brominated acrylonitrile-butadiene-styrene (ABS), polycarbonate (PC), and high impact polystyrene (HIPS) for the WEEE plastic. The temperature of 350 °C produced better results when considering acid value but presented lower bio-oil yields (38%) and high gas yields (42%). Catalytic upgrading experiments revealed the increased presence of polycyclic aromatic hydrocarbons (PAH) with an increase in viscosity of bio-oil, increase in char yield (from 11% to 24%), and decrease in gas yields (15% to 5%). Chemical composition showed presence of aromatic hydrocarbons such as styrene, methyl-styrene, and diphenyl-propane and nitrogenated compounds such as benzene-butane-nitrile, phenolic compounds, PAHs, and brominated compounds. WEEE plastic pyrolysis is a challenging subject due to contaminant presence and varying composition, and chemical composition

evaluation according to reaction time provides interesting insights into the evolution of semi-batch pyrolysis/catalytic upgrading experiments. Standardization and reproducibility of the tool should be conducted to continue the evaluation of pyrolysis and catalytic upgrading of a wide range of feedstocks.

**Keywords:** thermal cracking; reaction time; thermogravimetry; WEEE; e-waste; flame retardant ABS pyrolysis; PAH; physical–chemical properties; chemical composition

## 1. Introduction

### 1.1. E-Waste

Plastic waste poses a serious environmental problem, as it can take several years to decompose and pollutes terrestrial and aquatic environments [1–3]. In modern society, though, synthetic polymers are ubiquitous in the form of packaging, clothing, biomedical devices, electronic equipment, and household items, among others utilized by human society [1]. As of 2019, the average world consumption of plastics per capita was 60 kg/year, and the number has kept growing for over two decades. Even though 63% of world plastic waste is correctly disposed of in landfills (46%) or incinerated (17%), 22% is mismanaged or littered, and only 15% is collected for recycling [3]. Disposal in landfills can be a problem in some overpopulated and small areas due to extensive usage of space, and the more expensive process of incineration is used. The operation consists of burning the waste to reduce its size and volume. Intensive air pollution control is mandatory, and only about 20–25% of the energy produced by the reaction is recovered as electric energy [4]. Conversion of plastic waste into liquid fuels is an alternative recycling process where possibly more energy can be recovered with the same effectiveness in reducing waste volume [5–9].

Since most polymers are composed of hydrocarbon single units (monomer), it is possible to recycle waste plastics into liquid biofuels through pyrolysis or cracking processes [10–31], where the starting material is heated in an oxygen-deficient atmosphere to high temperatures (above 400 °C), breaking chemical bonds in the polymeric structure and producing smaller hydrocarbon molecules suited for use as liquid fuels [12,16,19,20]. In some cases, it is possible to obtain high yield of liquid fractions above 70% [10–12,14–16,20,23–25], and the hydrocarbon composition of initial feed reduces the need for catalyzed steps and/or further purification through separation processes and chemical reactions [12,13,17,19,25]. Nevertheless, it is desirable to control the degree of cracking in the pyrolysis reaction in order to be able to produce fuel within the specification range. This can be hard to achieve due to distillation of initial vapor products of the reaction if done in atmospheric pressure [32], so heavy-like fractions form such as waxes and heavy oils (C<sub>20</sub>–C<sub>30+</sub>) [11,12,17,19,21,24,25].

Plastic waste is a significant portion of urban municipal waste (MHSW), comprising 10–15% in weight of generated waste [33,34]. Considerable interest is being generated in coupling management of urban waste and energy generation through thermochemical conversion processes such as pyrolysis and gasification, achieving higher efficiencies than directly burning solid fuel, thus generating less CO<sub>2</sub> per MJ of energy produced. Besides, waste gasification can be used to produce syngas (a mixture of CO, H<sub>2</sub>, CO<sub>2</sub>, H<sub>2</sub>O, and CH<sub>4</sub>) and, through its transformation, produce a wide array of chemicals and fuels [35]. Gasification is a complex process involving partial oxidation of starting materials into simple gases such as CO and H<sub>2</sub> using less-than-stoichiometric air and/or steam, and it is composed of several different reactions. Thermal pyrolysis reactions occur to a degree in gasifiers, and heavy liquid fractions produced (high molecular weight hydrocarbons and oxygenates) are serious contaminants in the gasification process, causing clogging, pressure drops, corrosion, and catalyst poisoning in upstream processing of reaction products [35]. Small quantities of inorganic compounds such as metals and oxides may also be present in

plastic waste, and its accumulation inside vessels and equipment can lead to corrosion and operational/maintenance problems in gasification plants [36].

Waste electric and electronic equipment (WEEE) is one of the fastest growing waste streams in the world, and a considerable amount of it is disposed of incorrectly in urban areas and landfills. Directives around the world encourage its reuse, recycling, and recovery [14]. It consists of a wide range of devices such as refrigerators, washing machines, electric domestic equipment, computers, keyboards, videogames, medical equipment, and others. It is estimated that 32 %wt of WEEE is composed of plastic polymers, mainly acrylonitrile-butadiene (ABS), polypropylene, polystyrene, polycarbonate, polyethylene terephthalate, and others [37]. Pyrolysis of plastic waste from WEEE can be one way to recycle part of it into useful products such as gaseous, liquid, and solid fuels, but they are often contaminated with bromine derived from flame retardants added to plastic [38–40]. This can be a problem when considering this plastic waste for transformation via gasification [36].

### 1.2. Catalytic Upgrading

Catalytic upgrading of pyrolysis vapors through utilization of a second stage of vapor-phase cracking is a promising technique to overcome problems associated with liquid fractions formed during thermochemical conversion of plastic waste into fuels and chemical feedstock [14,25,38,41–54]. Basically, it consists of contacting the vapors flowing out of a thermal pyrolysis process with a porous catalyst heated fixed bed. Active sites at the catalyst surface promote further cracking of molecules and/or specific reactions such as deoxygenation, desulfurization, denitrification, dehalogenation, and others like isomerization, aromatization, and condensation [44,49,52]. The necessary specific reactions depend on the composition of feed and desired product characteristics. Therefore, a diverse catalyst choice can be made to achieve the process design goals.

Catalytic upgrading of pyrolysis vapors of WEEE plastic was studied using zeolite catalysts as Y-zeolites [14,38], Beta-zeolites [53], and ZSM-5 [14,38,51,53]; metal catalysts (Ni and Fe) impregnated into ZSM-5 [44,52]; metal oxides [53]; and metal catalysts impregnated into MCM-41 [44,54]. The authors focused mainly on carbon number distribution of products and removal of contaminants such as Br or Cl. Until now, no Si–Al ash catalyst was tested for the upgrading of WEEE plastic pyrolysis vapors focusing on the catalyst effects on the chemical composition and physical chemical properties of obtained upgraded bio-oil changing with respect to reaction time. Even though some authors investigated catalyst-to-feed ratio (C/F) effects on product composition [25,42,43,47] and reaction time effects [48,49], only Nishino et al. studied those effects at a larger process scale [47], and the feedstock was not composed of WEEE. Aside from papers published analyzing effects of reaction time focused on studying chemical composition and conversion [48,49], no physicochemical analyses were done to check the effects of time on those properties. This work studied C/F ratio and reaction time effects on product composition and physicochemical characteristics of bio-oil produced by the upgrading (2-stage vapor cracking) of pyrolysis vapors obtained from casings of scrap computers (WEEE) on a semi-pilot scale.

Chemical composition and physical chemical properties' variation with reaction time is an interesting way of analyzing semi-batch pyrolysis processes, indicating how thermo-catalytic reactions change the composition of feed and of products facilitating the comparison, design, and scaling of catalytic upgrading pyrolysis. In previous work, we used similar analyses to study catalytic upgrading of waste fats [55,56], and the analysis can be compared to the one obtained in this work.

## 2. Materials and Methods

### 2.1. Methodology

The methodology applied to develop, analyze, and discuss the results of this work can be summarized by four separate tasks composed of: feed material pre-processing, catalyst preparation, upgrading experiments and sample collecting, and analysis of catalyst and

liquid product obtained. The process flowchart illustrated in Figure 1 summarizes tasks and analysis conducted.

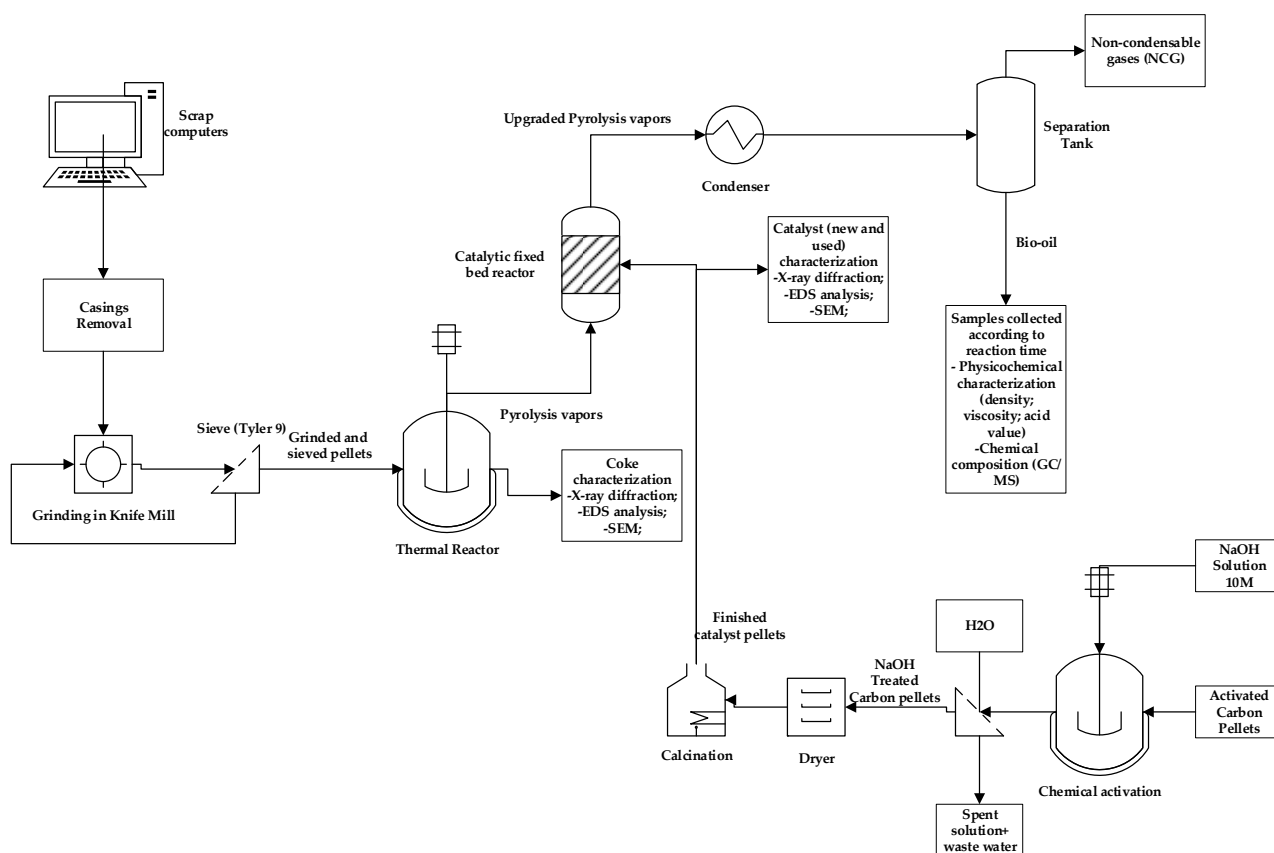


**Figure 1.** Process flowchart of catalytic upgrading of WEEE vapors using Si–Al ash catalyst pellets, in semi-pilot scale.

## 2.2. Materials

Scrap computers were obtained as the e-waste collected over the years in the building of the Institute of Technology (ITEC) located at Federal University of Pará (UFPA). They were composed of plastic material removed from old monitors, personal computers, and printers. The polymeric casings were manually removed and broken into smaller pieces to be fed into a knife mill, illustrated in Figure 2. The casings were ground in batches of 2 kg for 30 min. Afterwards, the ground WEEE plastic was sieved through a Tyler 9 mesh. The retained particles were subjected to grinding again and sieved until more than 95% of the initial material was ground to the desired particle size. Figure 3 shows WEEE before and after the grinding process.

For catalyst preparation, the carbon pellets used were commercial grade with an activated filter for water, and their specification follows in Table 1. NaOH 99% purity was utilized for preparation of the NaOH solution. Unless specified, all water utilized in these experiments and solution was deionized water.

The activated carbon was further treated with the concentrated NaOH solution in order to increase the mesopore size structure [57]. A detailed method for preparation of catalyst pellets was described in a previous work [55]. Briefly, the pellets were left in contact with two times their weight of concentrated (50% *w/w*) NaOH solution for 8 h. Afterwards, the pellets + spent solution mixture was separated using paper filters and washed with deionized water to remove excessive alkali until a pH of 10.0–11.0 was reached in water. The pellets were dried and calcined in a muffle (7LAB EQUIPAMENTOS E SERVICOS EIRELI ME, Rio de Janeiro, Brazil, Model Bio SEA—40 L) at 600 °C for 3 h at air atmosphere. After this process, the prepared catalyst contained even less carbon and can be called Si–Al

ash, as further analysis revealed that the pellets contained Si and alumina. The wastewater generated by the chemical treatment was neutralized with diluted sulfuric acid solution and discarded. For a scaled-up process, though, considerable optimization of NaOH solution concentration and quantity of wastewater generated would be needed, changing contact efficiency of the catalyst with an alkaline solution and possibly changing contact time. Even though catalyst quantities used for catalytic upgrading experiments are low (2.5–7.5 %wt), wastewater generated and its alkalinity would be unacceptable on a large scale.



**Figure 2.** Knife mill utilized for grinding WEEE plastic to adequate particle size to be fed into the pyrolyzer.



(a)



(b)

**Figure 3.** WEEE plastic before (a) and after grinding (b).

**Table 1.** Specifications of commercial grade carbon pellets for activation.

Specifications	Units
Particle size (mm)	3.9–4.1
Mean particle diameter (mm)	4.0
Surface area (m <sup>2</sup> /g)	900
Moisture (%)	5.0 (maximum)
Density (g/cm <sup>3</sup> )	0.45–0.55
pH	9.0–11.0

### 2.3. Experimental Procedure

The 2-stage catalytic cracking semi-pilot unit was well described in previous work [55,56]. Figure 4 presents a schematic diagram of said unit. Experiments were conducted using two types of investigation. First, thermal pyrolysis of WEEE plastic was done over a temperature range (300, 350, 400, and 450 °C) to evaluate product yields. For those experiments, the unit assembly was done using only the batch reactor (R-1) coupled directly to the condensing unit. There was no catalytic fixed bed. This was done to better evaluate process temperature dynamics and choose the temperature that gave better liquid yields for evaluation of the effect of catalyst quantity on product yields and composition. Studying chemical composition of the liquid fraction from thermal pyrolysis helps to understand what happens at the heated catalyst surface in the catalytic experiments, since the vapor composition fed to reactor R-2 should be very similar to the liquid fraction obtained in thermal pyrolysis. Afterwards, the catalytic fixed bed (R-2), composed of an electrically heated ( $P = 1.5 \text{ kW}$ ) stainless steel tube (length = 300 mm, i.d. = 15 mm), was coupled between thermal reactor R-1 and the condensing unit, and experiments were tested using different amounts relating to feed weight (2.5, 5.0, 7.5 %wt) of catalyst pellets so as to simulate longer residence times of vapors in contact with the catalyst at R-2. Even though the electrical heater can supply heat to the entire length of the tube, only the volume occupied by heated catalyst is counted as the catalyst fixed bed, so a higher amount of catalyst corresponds to a bigger catalyst fixed bed.

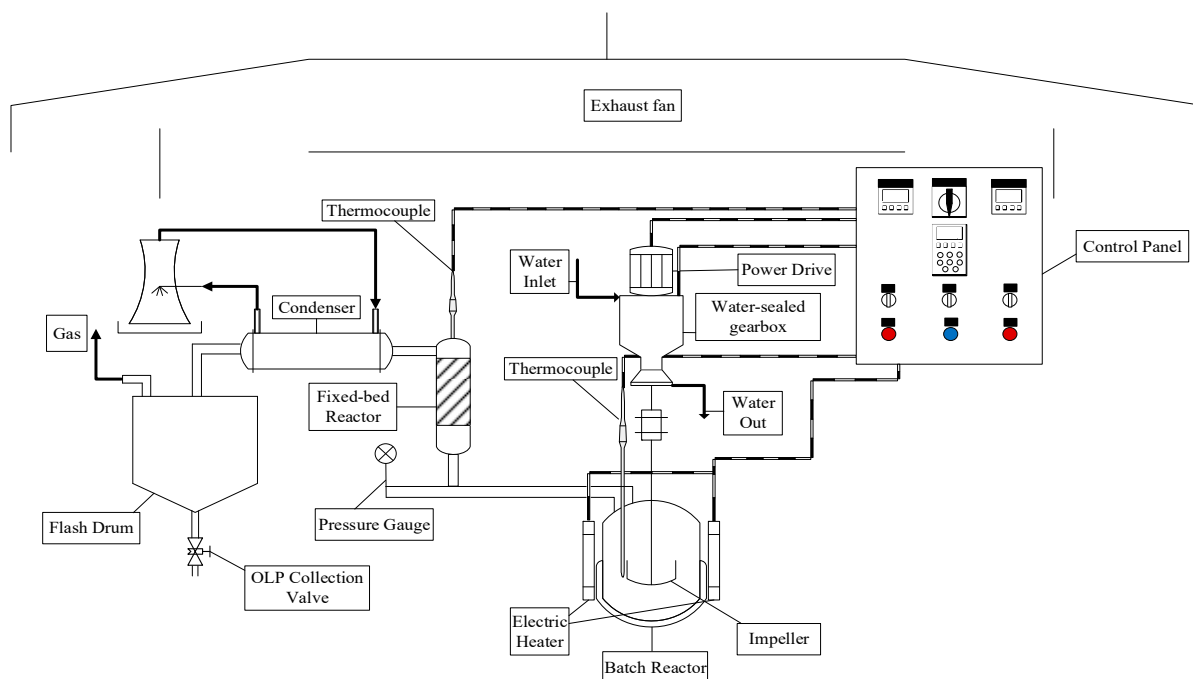


**Figure 4.** Schematic diagram of bench-scale stainless steel catalytic cracking reactor with a pyrolysis/batch reactor and a fixed bed reactor.

A typical run consisted of a few steps, very similar to both sets of experiments. For the thermal cracking experiments, first the unit was prepared by starting the condenser unit and allowing it to reach the desired temperature of 15 °C for the cooling water. Second, the water supply to the mechanical impeller seal was started and verified. Third, reactor R-1 was uncoupled from the system and the WEEE plastic (600 g) was fed manually to the inside of reactor R-1. Then, reactor R-1 was re-coupled to the system, taking care to correctly insert and adjust it to make sure that no gap was observed between the reactor and its cover or considerable torque would be observed in the impeller. As the feed is solid, it is harder to assemble the reactor when compared to feed liquids or semi-liquids as in our previous work [55,56]. The reactor was closed and coupled to the system using 8 sets of screws and

bolts having an internal diameter of 12 mm. Each set was composed of one screw and two bolts. The screw-and-bolts sets were assembled in pairs diametrically opposed to each other after securing one pair using a 16 mm tire iron. The subsequent pair was installed in a crosswise manner to the previously secured set in order to adequately close the reactor and avoid leakage of vapors in the reactor R-1. A graphite seal was also used between the reactor and its cover to further avoid leaks. After reactor setup, operating parameters were set on the control panel as impeller speed (100 rpm), desired final temperature, and heating rate (10 °C/min). To assist in monitoring and control of the process, operating parameters were recorded every 10 min. For each experiment done, the time and temperature of the initial flowing of vapors from reactor R-1 were recorded and samples were withdrawn after 15, 30, 45, and 60 min from the initial time of reaction (vapors flowing out of the vent) to evaluate product composition and physical—chemical characteristics with increasing reaction time. The non-condensable gases were vented or burned at the gas exit line. The reaction was deemed finished when there were no visible vapors flowing out of the gas exit line.

The catalytic experiments were done in similar manner in respect to feed and assembly of reactor R-1, with added steps to set up the catalytic fixed bed reactor R-2. After assembly of reactor R-1, catalyst pellets were added to uncoupled reactor R-2. Glass wool was used before and after catalyst pellets to help secure them and make the vapors flow more evenly through the catalytic fixed bed. The R-2 thermocouple was then inserted and the reactor was coupled to the system. High temperature rubber seals were used between each flange to avoid leaks in the system. After reactor R-2 setup, operating parameters were set on the control panel for the desired R-2 temperature and heating rate (10 °C/min). It is important to pre-heat the reactor to properly achieve desired pellet temperature before vapors flow out of reactor R-1 and to avoid temperature drop as, initially, cooler vapors come in contact with heated pellets. Because of this, reactor R-2 temperature was controlled initially at 20–30 °C higher than the desired set points.

#### 2.4. Feed Characterization

WEEE plastic was characterized separately with thermogravimetry (TG) analysis for each plastic waste collected (personal computers, monitors, and printers) and for the final mix of the three types. The TG analysis was done on a thermal scale (DTG-60H, Shimadzu, Tokyo, Japan) from 20 to 800 °C using a mass of 5 mg in air atmosphere inside a platinum crucible, using a 10 °C/min heating rate and a gas flow of 5 mL/min.

#### 2.5. Physicochemical and Chemical Composition of Bio-Oil

##### 2.5.1. Physicochemical Characterization of Bio-Oil

Characterization of bio-oil was done by measuring its density, kinematic viscosity, and acid value. Density was measured using a methodology adapted from standard method AOCS CC 10c-95 using a 5 mL glass pycnometer calibrated with distilled water. Kinematic viscosity was obtained according to adaptation of standard method ASTM D2515 on a temperature-controlled 40 °C thermostatic bath using manual suction. Time was measured manually using a chronometer, and three replicates were done for each sample. Cannon–Fenske viscosimeters of  $n^{\circ}$  50, 200, and 300 were used depending on estimated viscosity range of samples, and viscosity was determined using the lower bulb. The acid value was determined by titration of 0.2 g of sample dissolved in 50 mL of combined isopropanol/toluene solvent (50/50 %wt/.wt) with 0.1 N KOH standard solution and phenolphthalein as the acid–base indicator. The acid value titration method was adapted from AOCS Cd3d-63 [55,56].

##### 2.5.2. Chemical Composition of Bio-Oil

Chemical composition of bio-oil was obtained through GC–MS analysis as detailed elsewhere [58] on a gas chromatographer (CG-7890B, Agilent Technologies, Santa Clara, CA, USA) coupled to a mass spectrometer (MS-5977A, Agilent Technologies). A fused

silica SLBTM-5ms capillary column (30 m × 0.25 mm × 0.25 μm) was used. The sample injector was set at a temperature of 250 °C with a heating rate of 10 °C/min. 1.0 μL of sample was injected in split mode (1:50). The carrier gas flowrate used was 6.0 mL/min. The column temperature was increased from 60 to 280 °C. The detector was set to 230 °C and the quadrupole temperature was set to 150 °C. The concentrations were expressed in area, as no internal standard was used for comparison of the peak areas.

## 2.6. Characterization of Si–Al Ash Pellets and Chars

### 2.6.1. SEM and EDX Analysis

The morphological characterization of the Si–Al ash pellets' surface was performed by scanning electron microscopy using a microscope (Tescan GmbH, Brno, Czech Republic, Model: Vega 3) with 338×, 838×, 1.67k×, 3.33k×, 5.00k×, and 6.67k× magnifications. To prepare samples for analysis, coating with a thin layer of gold was done in the samples using a Sputter Coater (Leica Biosystems, Nußloch, Germany, Model: Balzers SCD 050). Elemental analysis and mapping were carried out by energy dispersive X-ray spectroscopy (Oxford instruments, Abingdon, UK, Model: Aztec 4.3).

### 2.6.2. XRD Analysis

The presence of crystalline phases in catalysts and chars was analyzed by X-ray diffraction (Rigaku, Japan, Model: MiniFlex600) at the Laboratory of Structural Characterization (FEMAT/UNIFESSPA). Generator power was 600 W with Cu-tube voltage of 40 kV and current of 15 mA, scanning range of 0.01 to 100° (accuracy = 0.02°), and high-speed silicone tape as the detector.

### 2.6.3. XRF Analysis

X-ray fluorescence spectrometry was conducted to better identify the composition of catalyst pellets and chars obtained. A WDS spectrometer (PANanalytical, Malven, UK, Model Axios Minerals) equipped with a ceramic X-ray tube and a rhodium (Rh) anode was used, and the maximum power level was 2.4 KW. The sample was prepared using 0.5 g of sample, 0.15 g of agglomerant (paraffin), and 3.0 g of substrate material pressed with a 25 ton charge. SuperQ Manager v5.3 software was used to acquire and treat data.

## 2.7. Mass Balances and Calculation of Yield of Reaction Products

The feed weight was recorded before loading the reactor. Each time, a fraction of the bio-oil obtained was weighed and added up to find the total mass of bio-oil obtained. After cooling, reactor R-1 was unmounted and the char was removed and weighed. The mass of gas was calculated by an integral global mass balance considering the whole semi-pilot unit as the control volume. Integral mass balances are better for analyzing batch or semi-batch processes. Integral mass balances are obtained by integrating a differential mass balance done on the system. Equation (1) describes differential mass balance:

$$\frac{dM}{dt} = \dot{M}_I - \dot{M}_O + G - C \quad (1)$$

where  $\dot{M}_I$  and  $\dot{M}_O$  are mass flow rates in and out of the delimited control volume, respectively.  $G$  and  $C$  are terms corresponding to generation and consumption of chemical species by existence of chemical reactions. Even though pyrolysis consists of a variety of chemical reactions, for global mass balances, there is no mass generation or consumption, those terms being important only when one considers a particular chemical species inside the control volume. For global mass balance,  $G - C = 0$ , and Equation (1) becomes:

$$\frac{dM}{dt} = \dot{M}_I - \dot{M}_O \quad (2)$$

Multiplying Equation (2) by  $dt$  and integrating, Equation (3) is obtained:

$$\int_{t_i}^{t_f} \frac{dM}{dt} dt = \int_{t_i}^{t_f} \dot{M}_I dt - \int_{t_i}^{t_f} \dot{M}_O dt$$

$$M_{t_f} - M_{t_i} = \int_{t_i}^{t_f} \dot{M}_I dt - \int_{t_i}^{t_f} \dot{M}_O dt \quad (3)$$

where  $M_{t_f}$  corresponds to material remaining in the reactor R-1 at the final time of reaction,  $t_f$ ; in this case, the char residue remaining in the reactor,  $M_{char}$ .  $M_{t_i}$ , is the initial mass in reactor R-1, corresponding to the mass of WEEE plastic loaded into reactor R-1,  $M_{feed}$ . There is no mass flow rate being added to the control volume, so  $\dot{M}_I = 0$ .  $\dot{M}_O$  corresponds to mass flow rates flowing out of the designed control volume, and it represents the pyrolysis vapors flowing out of reactor R-1 and going to the condenser, where it is separated into two fractions,  $\dot{M}_{bio-oil}$  and  $\dot{M}_{gas}$ , so  $\dot{M}_O = \dot{M}_{bio-oil} + \dot{M}_{gas}$ . Substituting these parameters in Equation (3), Equation (4) is obtained.

$$M_{char} - M_{feed} = - \left[ \int_{t_i}^{t_f} \dot{M}_{bio-oil} dt + \int_{t_i}^{t_f} \dot{M}_{gas} dt \right]$$

$$M_{feed} - M_{char} = \int_{t_i}^{t_f} \dot{M}_{bio-oil} dt + \int_{t_i}^{t_f} \dot{M}_{gas} dt \quad (4)$$

Assuming that mass flow rates of bio-oil and gases are constant, rearrangement of Equation (4) yields the final form of global mass balance for the semi-pilot unit of catalytic upgrading on Equation (5).

$$M_{feed} - M_{char} - M_{bio-oil} = M_{gas} \quad (5)$$

Weighing the amount of feed, solid char, and bio-oil obtained allows for calculating the mass of non-condensable gases evolved from the semi-pilot unit. Since the amount of gas is indirectly calculated, care must be taken to correctly measure feed, bio-oil, and char weights, because any fluctuation in these measured quantities will reverberate in gas yields obtained. The solid char corresponds to just the remaining solid residue of reactor R-1, due to the difficulty in accurately weighing the recovered catalyst pellets at the end of experiment runs; more often than not, the weight of catalyst pellets was lower after runs, due to fragmentation and loss of pellets in the gas stream or during disassembling of the catalyst fixed bed. Since catalyst loading is lower than 10% of the feed, this loss was assumed to be negligible. The yields of reaction products are calculated in relation to feed weight as follows:

$$Y_{bio-oil} [\%] = \frac{M_{bio-oil}}{M_{Feed}} \times 100 \quad (6)$$

$$Y_{char} [\%] = \frac{M_{char}}{M_{Feed}} \times 100 \quad (7)$$

$$Y_{gas} [\%] = \frac{M_{gas}}{M_{Feed}} \times 100 \quad (8)$$

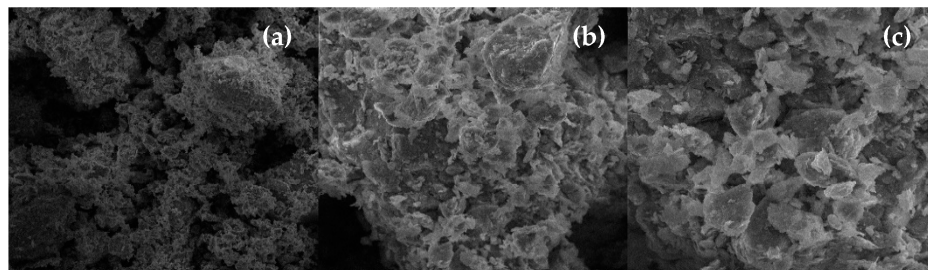
### 3. Results

#### 3.1. Characterization of the Catalyst

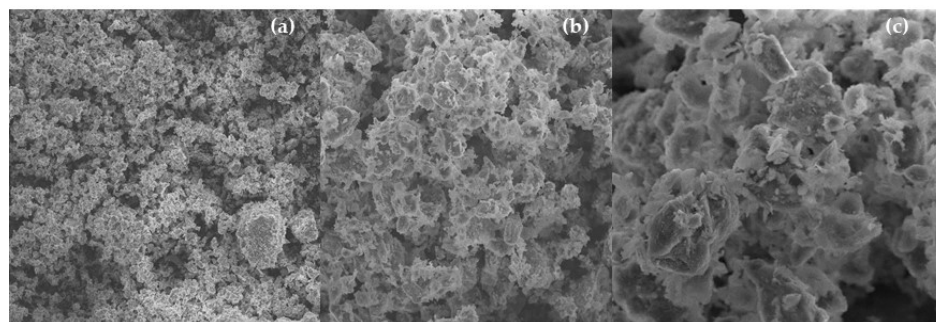
##### 3.1.1. SEM Analysis

Figure 5a–c are different magnifications ( $838\times$ ,  $3300\times$ , and  $6670\times$ ) of pellets before any chemical activation process was done. It can be seen that it exhibits a highly porous structure already as per specifications provided in Table 1 of  $900 \text{ m}^2/\text{g}$ . Higher magnification ( $6670\times$ ) reveals the presence of flat-shaped flakes of irregular order. After chemical activation, SEM images depicted in Figure 6a–c show presence of cavities with sizes between 4.0 and

10.0  $\mu\text{m}$ . By comparing the SEM images depicted in Figures 5 and 6, the effects of treating pellets with a high concentration NaOH solution can be seen. The chemical activation treatment provided more depth to the porous structure and reduced flake sizes. Tseng et al. described how concentrated NaOH solution could be used to increase porosity and surface area of activated carbons and even control it to some degree [57]. The effects of the activated carbon used in this work were not quite as effective as the ones in Tseng et al.'s work [57], probably due to chemical activation being done on the whole pellets as opposed to being done with char powder. The SEM images of Si–Al ash pellets after upgrading of WEEE plastic pyrolysis vapors illustrate the carbon deposition that occurred on the porous surface of catalyst due to gas–solid reactions occurring as pyrolysis vapors flow through the catalyst fixed bed, as shown in Figure 7c and corroborated in Table 2 concerning EDX analysis, as coke deposits form on the surface of catalysts by polymerization of aromatics present in the pyrolysis vapors or during reaction at the gas–solid interface [59]. In fact, Si–Al ash pellets, which were brick red after calcination, became black after catalytic upgrading experiments due to the carbonization that takes place inside the pores of the Si–Al ash catalyst.



**Figure 5.** SEM of virgin pellets [MAG: 838 $\times$  (a); MAG: 3.33k $\times$  (b); MAG: 6.67k $\times$  (c)].



**Figure 6.** SEM of Si–Al ash pellets [MAG: 338 $\times$  (a); MAG: 1.67k $\times$  (b); MAG: 5.00k $\times$  (c)].

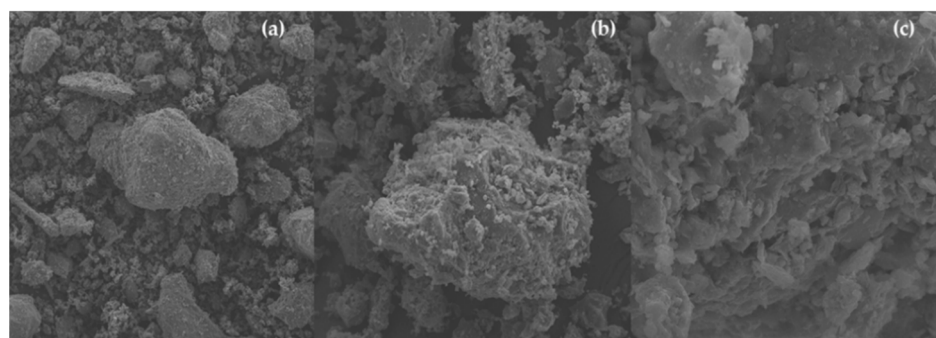


**Figure 7.** SEM of Si–Al ash pellets after catalytic upgrading of WEEE plastic pyrolysis vapors [MAG: 838 $\times$  (a); MAG: 3.33k $\times$  (b); MAG: 6.67k $\times$  (c)].

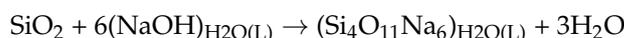
**Table 2.** Percentages in mass and atomic mass of virgin pellets, Si–Al ash pellets, and pellets after upgrading experiments.

Chemical Elements	Catalyst								
	Virgin Pellets			Si–Al Ash Pellets			Used Si–Al Ash Pellets		
	Mass [%wt]	Atomic Mass [%wt]	SD	Mass [%wt]	Atomic Mass [%wt]	SD	Mass [%wt]	Atomic Mass [%wt]	SD
C	-	-	-	-	-	-	43.28	56.58	0.37
O	58.21	72.00	0.11	61.67	74.58	0.08	31.67	31.08	0.30
Mg	0.94	0.77	0.02	1.01	0.80	0.02	0.30	0.19	0.02
Al	10.93	8.02	0.04	10.77	7.73	0.03	4.20	2.44	0.04
Si	22.49	15.85	0.07	17.88	12.32	0.04	8.67	4.85	0.07
K	2.05	1.04	0.02	1.93	0.96	0.01	1.18	0.47	0.02
Ca	1.40	0.69	0.01	1.72	0.83	0.01	4.84	1.90	0.04
Fe	3.07	1.09	0.02	2.20	0.76	0.01	3.50	0.98	0.04
Ti	0.45	0.19	0.01	0.49	0.20	0.01	0.23	0.08	0.01
Na	0.40	0.34	0.03	1.82	1.53	0.02	2.05	1.40	0.04
Mn	0.06	0.02	0.01	0.05	0.02	0.01	0.08	0.02	0.01

SD = Standard Deviation.

### 3.1.2. EDX Analysis

Table 2 show results from the elemental analysis conducted by dispersive X-ray energy for virgin, ready, and used pellets on the catalytic upgrading of WEEE plastic pyrolysis vapors. According to this analysis, pellets are composed of oxygen (58.21%), Si (22.49%), and Al (10.93%), suggesting composition of silicates ( $\text{SiO}_x$ ) and alumina ( $\text{Al}_2\text{O}_3$ ). Chemical treatment with concentrated sodium hydroxide lowered levels of Si as expected. Silicates react with NaOH, producing a soluble compound and water as per the following chemical reaction [60]:



This reaction is responsible for the increase in surface area and catalyst porosity, facilitating access of pyrolysis vapors inside the pores and active sites of the catalyst. There was a slight increase in sodium levels, probably due to adsorption and impregnation of some active sites with sodium oxide hydrates, also shown in the XRD analysis of Figure 8. After upgrading experiments on WEEE plastic pyrolysis vapors, coke deposits formed, increasing carbon content to 43.28%. The high carbon deposition suggests rapid deactivation of the catalyst, a troubling indication for packed bed operations, since the catalyst would need costly regeneration routines and generate unsecure conditions due to the possibility of plugging of the catalyst fixed bed with a dangerous pressure increase in the vessels. Considering semi-batch operations, whole batches could suffer from bad quality due to a recently deactivated catalyst. The authors wrote about reasons for catalyst activity loss in bio-oil upgrading experiments. In general, there are two main methods of catalyst deactivation: one is reversible deactivation over time, and the other is irreversible deactivation over regeneration cycles [61–64]. Oxygenated compounds like acids cause generation of coke deposits on active sites of metal oxide, and the coating of active sites results in loss of activity by preventing vapors access to the inside surfaces of the catalyst, causing reversible deactivation. Regeneration of the catalyst through burning of carbon deposits is then possible, but subsequent regeneration cycles tend to cause irreversible deactivation through sintering and poisoning of the catalyst active site at high temperatures required for regeneration [61,62]. The appearance of carbon deposits also shows that vapors could reach the insides of pores and active sites of catalysts, since coke-forming reactions tend to occur in later stages of cracking [59,65].

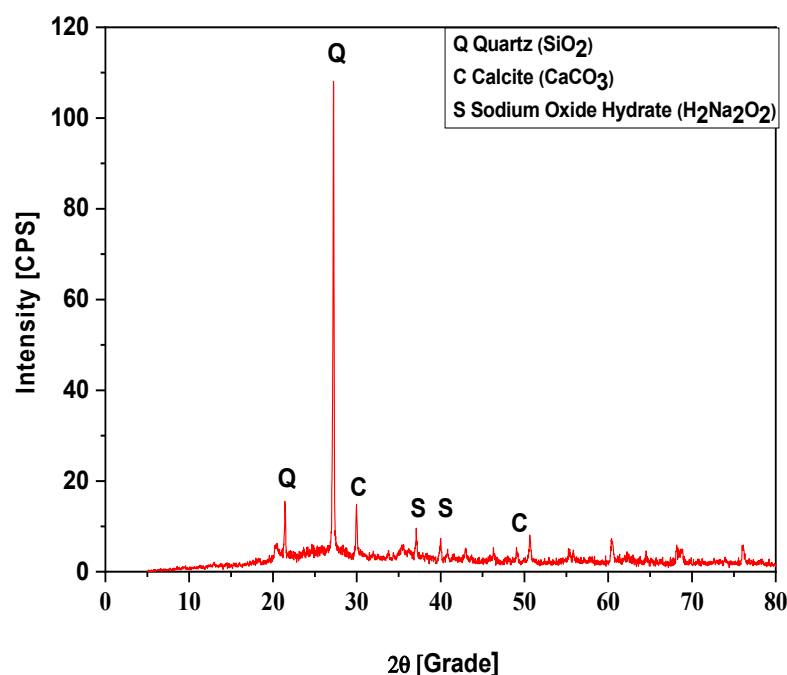


Figure 8. XRD of Si–Al Ash catalyst pellets.

### 3.1.3. XRD Analysis

The XRD diffractogram of the chemically treated pellets is shown in Figure 8. Three crystalline phases were observed, in accordance with the EDX analysis shown in Table 3, showing peaks for Quartz ( $\text{SiO}_2$ ) at positions  $2\theta$ : 26.6 and  $2\theta$ : 20.8; calcite ( $\text{CaCO}_3$ ) peaks at position  $2\theta$ : 29.4 and another of low intensity at position  $2\theta$ : 48.6; and sodium oxide hydrate ( $\text{H}_2\text{Na}_2\text{O}_2$ ) showed 2 peaks on positions  $2\theta$ : 37.1 and  $2\theta$ : 40.8. As was determined by EDX analysis (Table 3), pellets are composed of silica ( $\text{SiO}_2$ ), and the NaOH treatment added some crystalline phases to the catalyst structure like calcite and sodium oxide, formed by residual NaOH present in catalyst pellets after calcination. Figure 9 shows the XRD diffractogram of carbon pellets after upgrading experiments of WEEE plastic bio-oil, suggesting that heating and contact with pyrolysis vapors had little effect on the present crystalline phases. Even though EDX and SEM analysis revealed presence of carbon deposits (coke), DRX analysis could not show crystalline phases for carbon. No leaching of the mineralogical part of the pellets was done, so it is hard to observe peaks for graphitic carbon in the catalyst sample.

Table 3. Composition of chemically Si–Al ash pellets used as the catalyst for catalytic upgrading experiments, obtained via XRF fluorescence.

Component	%.wt/.wt
$\text{SiO}_2$	44.01
$\text{Al}_2\text{O}_3$	15.59
$\text{Fe}_2\text{O}_3$	6.28
CaO	5.21
MgO	1.19
$\text{TiO}_2$	0.95
$\text{P}_2\text{O}_5$	0.12
$\text{Na}_2\text{O}$	3.92
$\text{K}_2\text{O}$	2.14
Fire loss	20.59

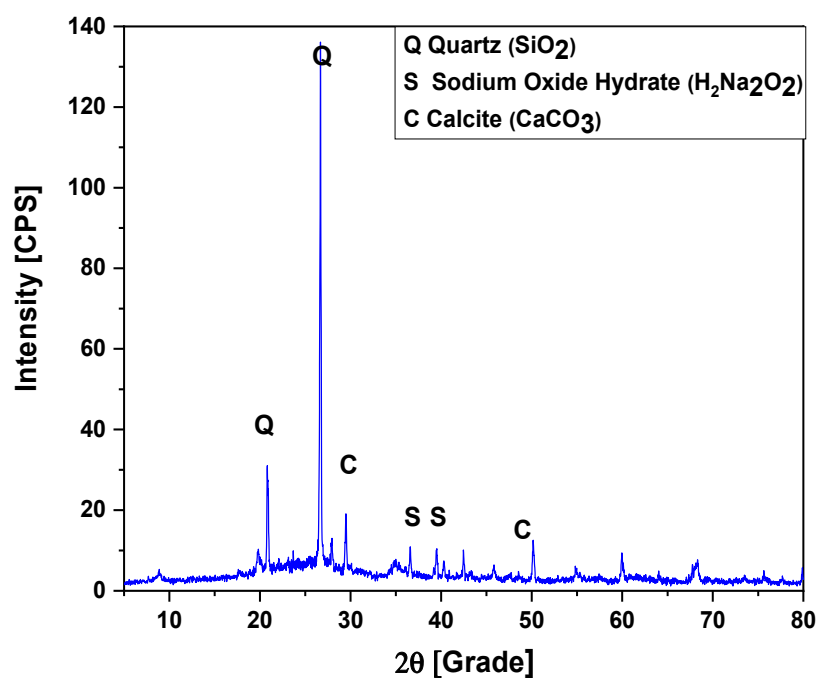


Figure 9. XRD of Si–Al Ash pellets after upgrading experiments.

#### 3.1.4. XRF Analysis

The XRF analysis of the Si–Al Ash pellets is presented in Table 3 and confirms the presence of  $\text{SiO}_2$  with 44.0 %wt, 15.6 %wt  $\text{Al}_2\text{O}_3$ , 6.0 %wt of  $\text{Fe}_2\text{O}_3$ , and calcium oxide 5.2 %wt. The sample showed 20.6% weight loss in the fire loss experiment, revealing it to be composed of a largely inorganic matrix. As hinted at earlier by elemental analysis of Table 3, the prepared catalyst contains minimal amounts of carbon and, after calcination in air atmosphere at 600 °C, most carbon content was burned or decomposed; the remaining ash was composed of silica and aluminum oxides, effectively being the catalyst used.

#### 3.2. Feed Characterization (TG Analysis)

Due to the nature of the WEEE plastic used in the thermal and catalytic experiments, a TG analysis was conducted for each material comprising the plastic waste. Figure 10 corresponds to the TG analysis done for monitors, PCs, printers, and a mix of them. The TG analyses were compared to analysis of pure samples of polymers commonly used as casings for computer-related paraphernalia, such as high impact polystyrene (HIPS), acrylonitrile-butadiene-styrene copolymer (ABS), polycarbonate (PC), and polyvinylchloride (PVC) [40].

It can be observed that all three computer parts composing the mix have distinct weight loss patterns. The monitors' TG show one peak of weight loss at around 400 °C. Hall et al. analyzed samples of computer monitors through TG analysis and found a similar pattern of one peak decomposition for all three different samples analyzed. They concluded the material was composed of ABS copolymer [40]. The early decomposition of CPU cabinets could mean the presence of flame retardants as brominated compounds or PVC [66]. Polycarbonate exhibits decomposition at higher temperatures, around 450–500 °C, and PC/ABS blends show similar decomposition patterns as the printers in this work [67]. The high temperature decomposition peaks observed for the materials could mean presence of polycarbonate. Roussi et al. commented about the fact that blends of polymers can degrade at lower temperatures due to radicals formed on thermal decomposition, initiating further degradation [68]. Indeed, thermal pyrolysis was initiated at low temperatures, and a high amount of gases was obtained. Jung et al. conducted thermal pyrolysis of brominated ABS (Br-ABS) on a fluidized bed reactor and obtained similar results to those of this work, with respect to chemical composition of bio-oil, yields, and TG analysis, even though the system used was largely different [69]. The mix of the three different computer

plastics showed a pattern of weight loss combining the three other materials comprising the feedstock, obviously. Degradation of combined samples initiated with lower temperatures and the pyrolysis experiments showed the same behavior, confirming the presence of flame retardants or PVC. The GC/MS analysis could not identify chlorinated compounds but showed the presence of brominated compounds in minor fraction as bromophenols.

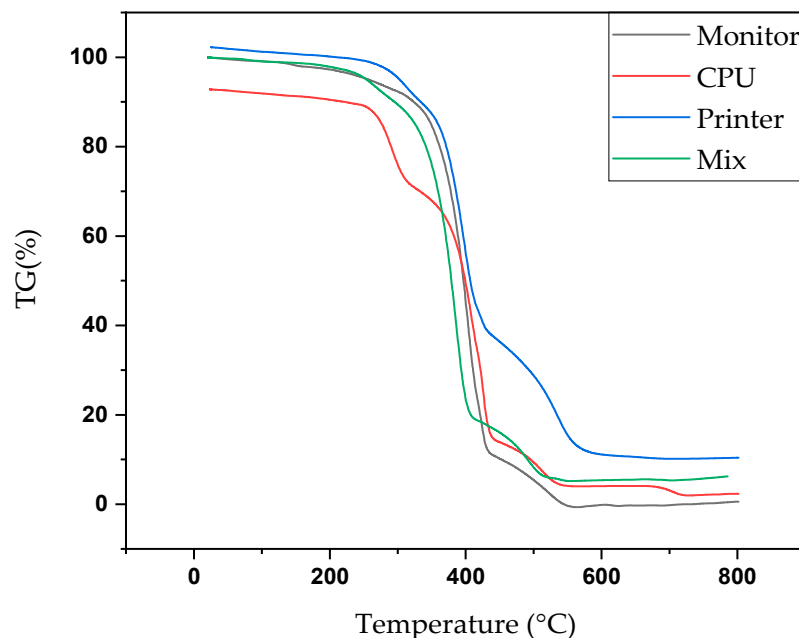


**Figure 10.** TG analysis of different computer parts comprising the mixed WEEE plastic feed used for thermal and catalytic cracking experiments.

### 3.3. Investigation of Thermal Cracking of WEEE Plastic

#### 3.3.1. Mass Balance and Yield of Reaction Products

As it was stated previously in Section 2.3, first an investigation was done on thermal cracking of WEEE plastic, without a catalyst fixed bed, over a determined range of temperature (350–500 °C) to evaluate process conditions, yields, chemical composition of bio-oil, and time evolution of the process. Table 4 shows process parameters and yields obtained over the temperature range used on thermal cracking.

**Table 4.** Mass balance and yields of reaction products of thermal cracking of WEEE plastic over the temperature range of 350–500°C.

Process Parameters	Temperature [°C]			
	350	400	450	500
Mass of plastic waste [g]	600.5	600.5	600.5	615.0
Cracking time [min]	120	120	120	120
Mass of solids (coke) [g]	115.1	128.8	149.8	112.5
Mass of liquids (OLP) [g]	232.9	357.0	382.5	393.1
Mass of gas [g]	252.5	114.7	68.2	109.4
Yield of liquids [%]	38.78	59.45	63.70	63.92
Yield of solids [%]	19.17	21.45	24.94	18.29
Yield of gas [%]	42.05	34.22	11.36	17.79

Table 4 shows yields of bio-oil and char increasing with temperature, while that of gaseous products reduces, as depicted graphically in Figure 11. Bio-oil yields increased by 64.82% at 500 °C in relation to the initial bio-oil yield of 38.78% at a temperature of 350 °C. Bio-oil yields are consistent with what is found in the academic literature [70,71].

Jung et al. [70] pyrolyzed high-impact polystyrene (HIPS) and acrylonitrile-butadiene-styrene (ABS copolymer) in a fluidized bed fast pyrolysis reactor and found yields ranging from 70–87% for HIPS and 62–84% for ABS over a temperature range of 410–550 °C. The higher yields of liquids are probably due to a more efficient heat transfer obtained by fluidized bed fast pyrolysis when compared to a fixed bed reactor (slow pyrolysis). Slow pyrolysis reactors, such as the electrically heated fixed bed reactor utilized in this work, show lower heat transfer rates (especially when pyrolyzing solid material) than fluidized bed fast pyrolysis reactors. Lower heat transfer rates are associated with lower bio-oil yields and higher solid fraction (char) yields for lignocellulosic biomass [72]. Even though there is large difference between polymeric material present in WEEE and lignocellulosic biomass, the same behavior is demonstrated here concerning heat rates and pyrolysis reactors. Studies showed that conventional fixed bed pyrolysis of ABS produces lower bio-oil yields when compared to fluidized bed fast pyrolysis of the same material [69,71], corroborating the same behavior for ABS containing polymers. Bhaskar et al. [71] pyrolyzed ABS copolymers in a laboratory scale fixed bed reactor and found liquid yields of 39%, consistent with the yields found in this work.

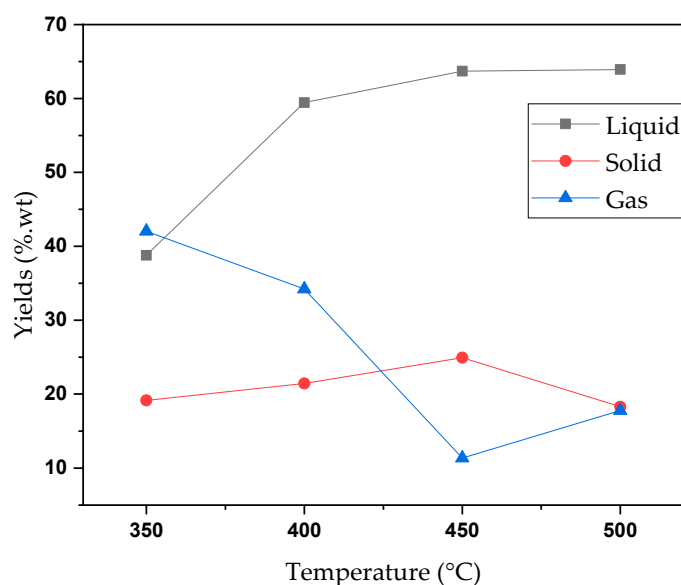


**Figure 11.** Effect of temperature on yields of products obtained through thermal cracking of WEEE plastics.

The plastic feed used in the semi-pilot unit showed a tendency to form gases and liquid products at low temperatures, as low as 200 °C, as evidenced by the TG analysis done in Figure 12, which shows small peaks of weight loss starting at 143 °C to 289 °C, with a combined weight loss of 9.7%. Some polymers containing flame retardants exhibit the tendency to depolymerize at low temperatures, including those found among WEEE plastics, such as ABS [69,71]. Normally, reactions occurring by thermal decomposition are endothermic and, because of this, reactor R-1 could only supply heat for occurring reactions, maintaining the reaction temperature until most products that had initially formed at the corresponding temperature had distilled to the condensing unit. Only then, would the reaction proceed and reach higher temperatures in reactor R-1. That said, the defined temperatures chosen correspond to the final temperatures reached and maintained until no more vapors or liquid products could be collected. This is why we decided to investigate lower temperatures for the thermal cracking experiments, until the maximum designed temperature allowed for reactor R-1 of 500 °C.

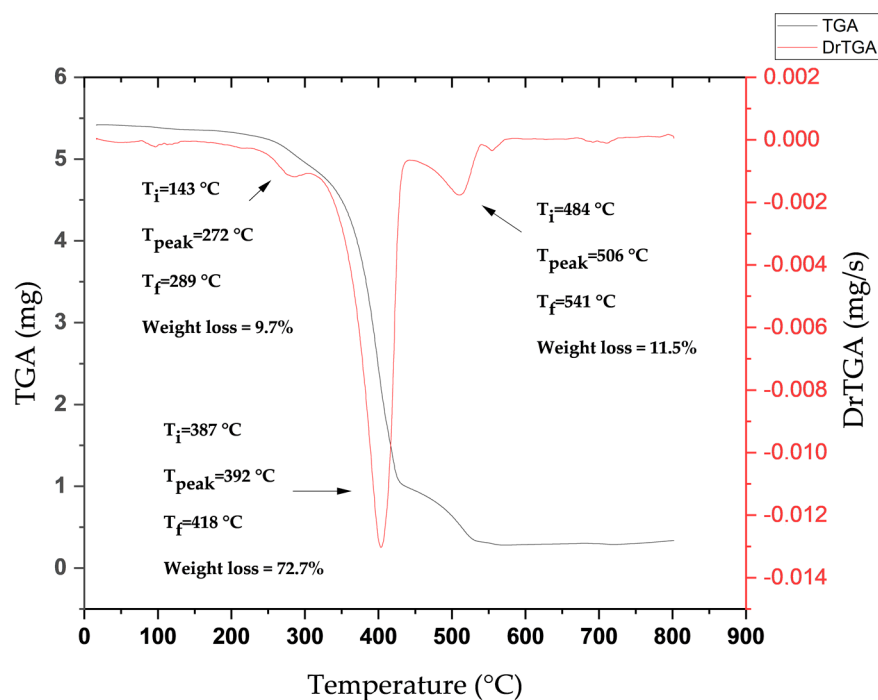


Figure 12. TG analysis of WEEE plastic feedstock.

At a first glance, temperature effects on bio-oil yields seem different from what is observed for most plastic feeds, where liquid fractions tend to decrease with increasing temperature [73–77]. Temperature is a key parameter affecting product yields [8], as higher temperatures are said to promote cracking reactions occurring along the polymeric chains of plastic feed. Additionally, temperature affects the initial products formed, producing smaller, more volatile substances, thus reducing yields of liquid bio-oil and solid fractions, but increasing gas quantity [73–77]. As was stated earlier, though, cracking reactions are endothermic and proper temperature control of such processes is no easy task, especially when considering a semi-batch fixed bed reactor. In order to control process temperature, one needs to design reactors and process parameters capable of supplying enough heat to overcome the energy needs of occurring endothermic reactions. Research focused on study temperature effects on yields of pyrolysis products achieve desired temperatures in a variety of ways, including using small quantities of feed [75,76,78], pressurized vessels [77], fluidized bed reactors with pre-heated inert beds [73], 2-stage vapor cracking [25], and high heating rates [75,76]. In our case, the reaction temperature indicates the extent at which the material was pyrolyzed, much like thermogravimetry analysis. The TG of Figure 12 shows the highest peak of weight loss between 400 and 450 °C, so one could make the assumption that liquid and/or gas yields increase until after that temperature range. In fact, bio-oil yields shown in Figure 10 increased until reaching a plateau at around 450–500 °C. The temperature range investigated is located around the zones with higher weight loss demonstrated by the TG analysis, so liquid yields tend to increase with increasing temperature. Studies focusing on temperature effects on plastic pyrolysis yields investigated higher temperatures (usually over 500 °C), having some sort of control over the degradation temperature used [73,74,76]. The studies investigating lower temperatures also found that liquid yields tend to increase until the 450–500 °C range [75,77,78]. Miskolczi et al. [79] reported the same behavior for flame retardant ABS polymer: liquid yields increasing in a temperature range of 360–440 °C.

Observing the TG analysis of Figure 12, it is expected that high yields of solid fraction would be obtained for temperatures below 400 °C, since little weight loss was observed (9.7%). Instead, solid yields remained in the range of 20% for all experiments, and a high yield of gases was achieved for 350 and 400 °C, of 42.05% and 34.22%, respectively.

This happened because experiments were conducted until no more vapors flowed out of reactor R-1. Temperatures were maintained on setpoints even when higher temperatures could be achieved and the time required to thermally degrade samples was constant throughout all experiments, as shown in Table 4. From previous work with the same unit [55,56], one can observe that solid fraction yields are influenced by the extent of reaction, i.e., low reaction times mean a higher yield of solids. Maintaining reaction at temperatures below the highest peak observed in the TG had a marked influence on gas yields, producing a high amount of gases. This differs considerably from other work, where low yields of gas were obtained for the pyrolysis of flame-retardant ABS using temperatures exceeding 400 °C [69–71,79]. Authors commented on the fact that flame retardant-ABS polymers can produce gases such as HCN and NH<sub>3</sub> for ABS at low temperature pyrolysis by cyclization of acrylonitrile units [79,80], and halogenated containing polymers like PVC produce HCl [76]. Brominated compounds are also thought to be produced at low temperatures for flame-retardant ABS [71]. Nitrogenated compounds accumulate in the liquid fraction of ABS pyrolysis [80], and low pyrolysis temperature programs can be one way of lowering these compounds' concentration in the bio-oil by producing N-containing gases. Brebu et al. conducted thermal degradation of ABS copolymers and found out that a programmed step of 300 °C for a set amount of time could reduce nitrogenated compounds in the bio-oil composition [80]. The pyrolysis process done in the semi-pilot unit differs considerably from the TG analysis with respect to temperature control when the desired setpoint temperature is lower than 450 °C. Due to the amount of WEEE plastic loaded into reactor R-1 and power supplied by the electrical heater (2.5 kW), the pyrolysis temperature could not reach values beyond 400 °C until most of the feed had cracked and vaporized. Therefore, only for the experiments done using setpoint temperatures of 350 °C and 400 °C could a desired temperature control around the reaction temperature be adequately maintained until no more vapors flowed out of the reactor. For experiments with a setpoint of 450 and 500 °C, the reaction temperature was increased using a heating rate of 10 °C/min until reaching cracking and flowing of vapors out of the reactor, and this was maintained until reaching 450 and 500 °C, respectively. The time of reaction was the same for all experiments, though, and seems to be related to feed weight loaded into reactor R-1. Maintaining reaction at lower temperature stages seems to have an effect on product quality, and further physical–chemical analysis shows that lower acid values were obtained for experiments done using 350 °C as the setpoint. Further analysis of gas composition should be done to evaluate this effect, and since gas quantity generated was measured by difference, fluctuations in weight readings of other variables can profoundly affect the gas yields. Details of low temperature cracking of WEEE plastics could be the subject of upcoming papers.

A black solid fraction remained as a residue inside the fixed bed reactor. This product can be classified as a charcoal or char, composed of amorphous and crystalline carbon, including a fraction of high boiling point hydrocarbon compounds such as polycyclic aromatic hydrocarbons (PAH) and aliphatic compounds with long carbon chains (C<sub>100</sub>–C<sub>200</sub>) [59]. PAH and the asphalt-like compounds of high carbon numbers are the last products formed by polymerization, aromatization, and condensation reactions that occur in later stages of cracking before turning into elemental carbon [59,65]. Even though there is considerable difference among structures of different polymers, the char formed presents a relatively consistent chemical composition throughout all plastic feedstocks; the quantity and composition of PAH and long chain hydrocarbons in char are dependent on variables like feedstock type, temperature, heating rate, time of reaction, and process design [81]. For instance, it is possible to conduct pyrolysis of plastic until little to no char is produced due to primary depolymerization reactions dominating the reaction mechanism, reducing the extent of aromatization, condensation, and polymerization forming the char precursors (PAH) [59,81]. The XRF analysis revealed that 91.0% was composed of carbon and 2.76% of bromine (Br), confirming that WEEE plastic is composed of flame-retardant Br-ABS. The XRD analysis of the obtained char in thermal experiments at 450 °C is presented in Figure 13.

No leaching of the mineralogical part was done to really take a look at the carbon structure present [82]; instead, the high peaks observed are due to inorganic components present, such as titanium dioxide, commonly used as a pigment for this type of plastic [83,84]. We also investigated presence of other types of inorganic flame retardants, such as  $\text{Sb}_2\text{O}_3$  [85]. Major peaks were found at positions  $2\theta$  of 25.6, 32.0, and 36.4°.

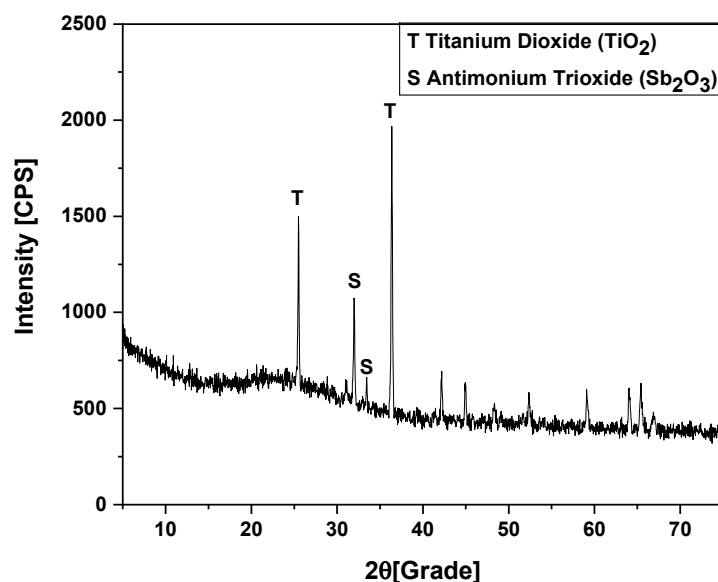


**Figure 13.** XRD analysis of char obtained through thermal cracking experiments at 450 °C of WEEE plastic.

Char yields showed a slight tendency to increase from 350 to 450 °C for our WEEE feedstock, in accordance with the academic literature, where higher temperature and residence time of remaining feed inside the reactor allow the reaction to reach the later stages, where condensation and polymerization reactions occur between reaction products [59]. Between 450–500 °C, the last decomposition peak showed by TG analysis occurs, possibly due to polycarbonate cracking [67]. Indeed, the char yield reduced from 450 to 500 °C, while the gas yield increased with no increase in the liquid fraction. Further investigation of this temperature range and gas analysis of the system could be the subject of upcoming papers.

### 3.3.2. Physical–Chemical Characteristics and Chemical Composition of Thermal Cracking Bio-Oil

The bio-oil obtained through thermal cracking had a standard aspect when considering plastic feedstock, being a dark liquid of acrid odor with some sort of green or red hue to it. As the bio-oil obtained was fractionated in samples given a predetermined reaction time, the weighted average of each physical chemical property was calculated using the individual values of measured properties and their respective mass of collected bio-oil at a given reaction time. The measured properties and their respective mass fractions are shown in Table 5 along with the weighted averages of properties at their respective run temperatures.

Mean density of bio-oil remained between 0.92–0.94 g/cm<sup>3</sup> and viscosity between 1.24–1.44 mm<sup>2</sup>/s. These values can be compared to other work in which the thermal degradation of commonly used plastics for WEEE was conducted. Plastics considered are HIPS, ABS, PC, and PVC. Brebu et al. conducted thermal degradation experiments of ABS on a fixed bed glass reactor at 450 °C and obtained densities of 0.89 g/cm<sup>3</sup> for the bio-oil [80]. The viscosities of the WEEE bio-oil showed values similar to other plastic feedstock pyrolysis oils. The bio-oil from plastic feedstocks shows lower viscosities when compared to other feeds, such as lignocellulosic material or lipid-based ones [55,56,58]. This is associated with the presence of aromatic compounds and volatiles, not commonly present for triglyceride material, in the case of thermal cracking. Plastic feedstock bio-oil

seems richer in compounds of higher volatility (gasoline range) while lipid-based ones present longer chain alkanes and alkenes (diesel range) [55,56]. The acid values shown in the samples are linked to the presence of acidic and oxygenated compounds. The chemical composition analysis showed the presence of phenolic compounds possibly related to the presence of polycarbonates in the composition of WEEE [67], probably responsible for a major fraction of acidity of the samples. The experiments done at 350 °C showed lower acidities and presented high gas yields, indicating the presence of decarboxylation reactions happening with those oxygenated compounds.

**Table 5.** Weighted average of determined physical–chemical properties and their respective measured properties of time fractions for thermal experiments.

Temperature (°C)	Reaction Time (min)	Bio-Oil Quantity (g)	Density (g/cm <sup>3</sup> )	Viscosity (mm <sup>2</sup> /s)	Acid Value (mg KOH/g)
350	15	96.5	0.92	1.30	26.9
	30	82.5	0.92	1.33	27.7
	45	53.9	0.92	1.44	27.5
	<b>Total</b>	<b>232.9</b>	<b>0.92</b>	<b>1.34</b>	<b>27.4</b>
	400	100.2	0.91	0.98	80.9
400	30	101.3	0.93	1.35	26.2
	45	98.2	0.94	1.38	31.7
	60	57.3	0.95	1.26	48.8
	<b>Total</b>	<b>357.0</b>	<b>0.93</b>	<b>1.24</b>	<b>46.7</b>
	450	103.2	0.91	1.46	33.0
450	30	95.5	0.98	1.36	24.8
	45	94.7	0.96	1.36	77
	60	89.1	0.91	1.32	28.3
	<b>Total</b>	<b>382.5</b>	<b>0.94</b>	<b>1.38</b>	<b>40.8</b>
	500	15	85.9	0.95	1.50
500	30	97.8	0.91	1.56	23.1
	45	150.3	0.92	1.38	18.1
	60	59.1	0.96	1.31	84.7
	<b>Total</b>	<b>393.1</b>	<b>0.93</b>	<b>1.44</b>	<b>54.7</b>

The chemical compositions of each time fraction was also determined by GC/MS and are available as tables in the Supplementary Materials. Mostly, the bio-oil is comprised of aromatic hydrocarbons such as benzene derivatives (benzene, 1,1'-(1,3-propanediyl)bis- and benzene(1-methylethyl)-); styrene derivatives (styrene and methyl-styrene); nitrogenated compounds derived from nitriles such as benzene–butane–nitrile and other nitrogenated aromatic compounds; and PAH such as ramified naphthalenes and phenolic compounds (phenol and cumenol). The thermal degradation of polymers is said to function on a random scission model [66], and the styrene and acrylonitrile derivatives are indicative of the feed matrix being composed of ABS, while the phenolic compounds formed indicate presence of polycarbonate material. No chlorinated compounds were detected in the GC/MS analysis, indicating that the feed material did not contain PVC. The high amount of nitrogenated compounds suggests that gas formed on the thermal experiments as nitrogen related gases HCN or NH<sub>3</sub> [79,80]. Those compounds detected were mainly formed by scission of bonds, but they could also be formed between highly reactive intermediary compounds formed during cracking. Benzene–butane–nitrile seem to be formed in the reaction between a styrene unit and acrylonitrile [71]. The chemical functions of each bio-oil obtained at different temperatures (350–500 °C) are presented as a function of reaction time in Figure 14.

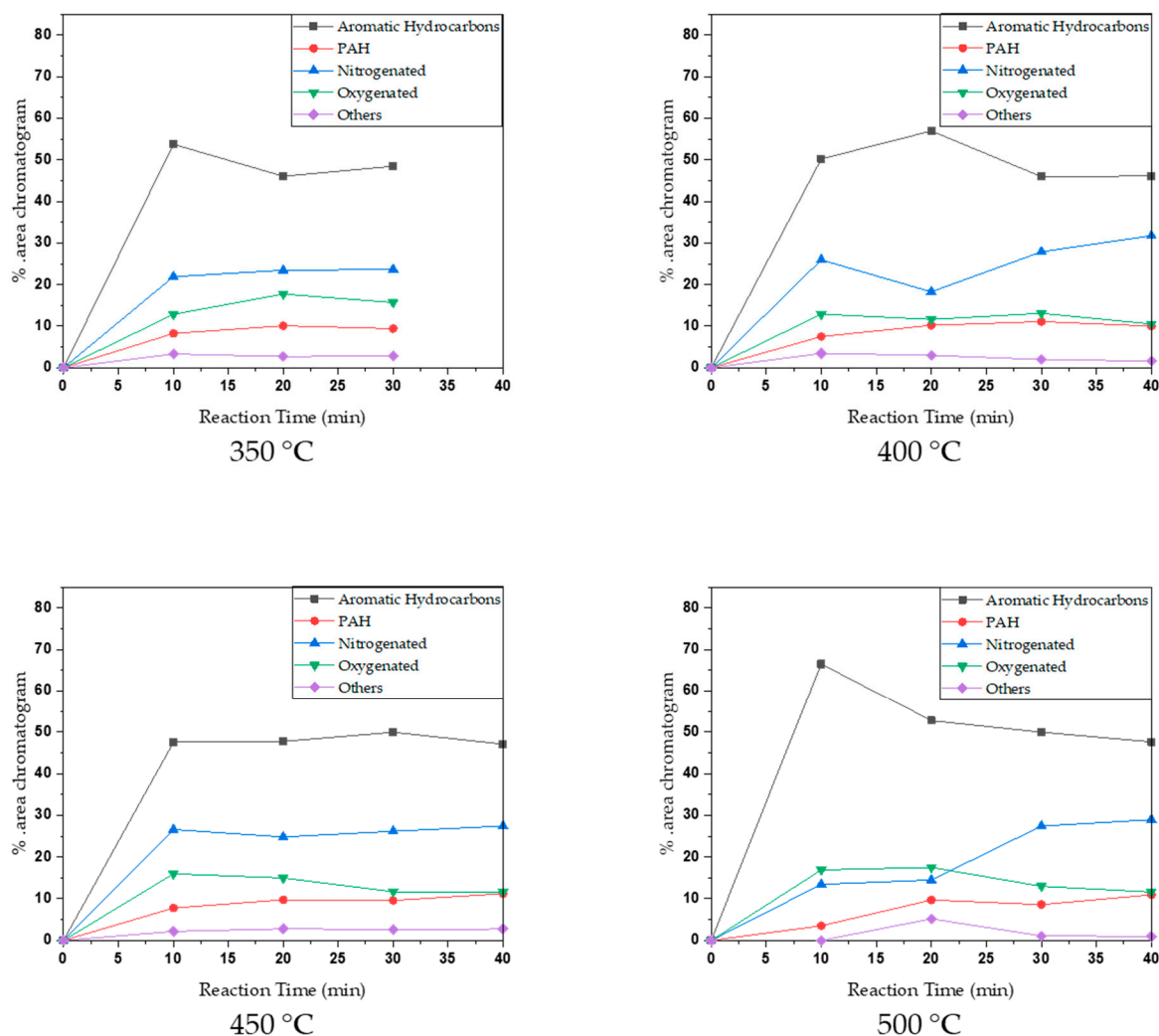


**Figure 14.** Time behavior of chemical functions present in thermal cracking of WEEE plastic at 350, 400, 450, and 500 °C.

The evaluation of chemical functions with reaction time revealed presence of aromatic hydrocarbons in the range of 45 to 70%; nitrogenated compounds as aromatic nitriles and benzene–butane–nitrile in the range of 20–30%; and the presence of PAH increasing with reaction time, indicating the evolution of cracking reactions until polymerization of aromatic compounds and formation of char. The oxygenated compounds were phenols and ketones, while the other fraction corresponds to non-identified compounds. The fraction of nitrogenated compounds seems to be related to the reaction temperature, increasing to the range of 30% for 400 °C and 500 °C. Lower fractions of nitrogenated compounds were obtained using 350 °C, and we already commented on the possibility of rejecting nitrogen in the gas stream as  $\text{NH}_3$  or  $\text{HCN}$ . Overall, the evolution of chemical function fractions of the thermal cracking experiments presented fairly constant compositions, despite being a semi-batch reactor where the feed composition changes as vapors are formed, suggesting that thermal decomposition of WEEE plastics occurs, forming the same chemical species throughout the entire reaction time, possibly due to uniform decomposition of the entire feed. Indeed, thermal decomposition of plastic polymers is said to function on a random radical scission model where the same smaller molecules are formed and vaporized continuously, consuming heat supplied by an electrical heater and maintaining the remainder of the feed almost unchanged [66]. This thermal decomposition behavior may explain why some polymers produce high yields of their respective monomers, such as decomposition of polystyrene generating high yields of styrene monomer [86].

A previous work using the same analysis in the same pyrolysis unit but using a different feedstock, waste animal fat [56], showed that chemical composition of bio-oil obtained through thermal pyrolysis suffers radical changes with reaction time, where initially the feed is largely composed of fatty acids and, in later stages of reaction, converts itself almost entirely to aliphatic hydrocarbons, indicating that the mechanism of thermal decomposition of lipid based materials follows a largely different route. Composition and physical–chemical analysis of fractioned samples of bio-oil considering reaction time is a powerful tool to analyze process evolution and even reaction mechanisms.

### 3.4. Upgrading of WEEE Plastic Pyrolysis Vapors over Chemically Treated Carbon Pellets

#### 3.4.1. Mass Balance and Yield of Reaction Products

After testing and acquiring some knowledge about thermal cracking of the WEEE plastic feedstock, the catalyst fixed bed was coupled and loaded with catalyst pellets to conduct experiments of catalytic upgrading using 2.5, 5.0, and 7.5 %wt. of the catalyst related to the weight of the feed at 450 °C. The reasons behind using 450 °C for the catalytic experiments include the excellent yield of bio-oil obtained in thermal experiments and consistency of chemical functions present in the bio-oil. In the case of upgrading experiments, the catalyst fixed bed was maintained at 450 °C at all times, even when the reactor was producing vapors at a low temperature. Table 6 presents the results of mass balance and yield of reaction products.

**Table 6.** Mass balance and yields of reaction products of catalytic upgrading of WEEE plastic pyrolysis vapors over catalyst fixed bed of 0.0, 2.5, 5.0, and 7.5 %wt at 450 °C.

Process Parameters	Catalyst Quantity [%wt]			
	0.0	2.5	5.0	7.5
Mass of plastic waste [g]	600.5	600.5	600.5	600.5
Cracking time [min]	120	120	120	120
Mass of solids (coke) [g]	149.8	70.5	104.6	148.3
Mass of liquids (OLP) [g]	382.5	437.7	417.2	418.4
Mass of gas [g]	68.2	92.3	78.6	33.8
Yield of liquids [%]	63.70	72.88	69.47	69.67
Yield of solids [%]	24.94	11.74	17.42	24.70
Yield of gas [%]	11.36	15.37	13.09	5.63

It can be observed that the use of the catalyst slightly improved bio-oil yields, while reducing gas and solid yields, when compared to thermal experiments done using 450 °C as the setpoint temperature. With respect to catalyst quantity, solid yields increased, while gas yields decreased. Bio-oil yields remained in the range of 70%. Muhammad et al. conducted catalytic upgrading experiments using a 2-stage vapor cracking reactor at 500 °C and obtained similar results for the degradation of ABS copolymers [14]. They used zeolite Y and HZSM-5 as catalysts with a C/F (catalyst-to-feed ratio) of 1. Hall et al. pyrolyzed Br-ABS in a fixed bed reactor containing zeolite Y and HZSM-5 as catalysts and found low yields of liquid in the range of 24–35% and a low quantity of gas. They used a C/F of 1 at 440 °C. A significant amount of coke was deposited on the surface of the catalysts [38]. Ma et al. conducted upgrading experiments with Br-ABS at 450 °C with different C/F ratios of 0.02, 0.2, and 0.4 using HZSM-5 and a Fe-loaded catalyst to determine influence on yields of products. They reported yields very similar to the ones obtained in this work, with over 80% of bio-oil yield and 13% for gas [52]. They commented on the fact that the high surface area provided by the catalyst and acidic sites contributed to plastic decomposition. The Fe catalyst with lower acidity than HZSM-5 promoted higher bio-oil yields since higher acidity contributes to gas formation. Indeed, gas yields tended to reduce with increasing catalyst content. The higher amount of char formed may be related to the increase in residence time of vapors inside the thermal reactor because of increased pressure due to the catalyst fixed

bed being in place. A similar effect was observed in previous experiments made using the same unit [55,56]. It is possible that some reflux occurs due to the increased pressure drop of the catalyst fixed bed being in place, affecting products in reactor R-1, including char quality and yields. The extent of the reflux, if any, is affected by the specific configuration used in the semi-pilot unit, where reactor R-2 is vertically positioned, increasing pressure drop through the catalyst fixed bed. This is also affected by the tube diameter of reactor R-2 and the shape of the packed bed particles, influencing how pyrolysis vapors flow through the catalyst bed. The surface area of catalyst pellets also increases residence time and contact with a hot surface. The increased residence time allows the reaction to reach the later stage, producing PAH and carbon, forming the residual char. Figure 15 presents the information in Table 6 in the form of chart for better insight into the effect of catalyst quantity on the yield of reaction products.

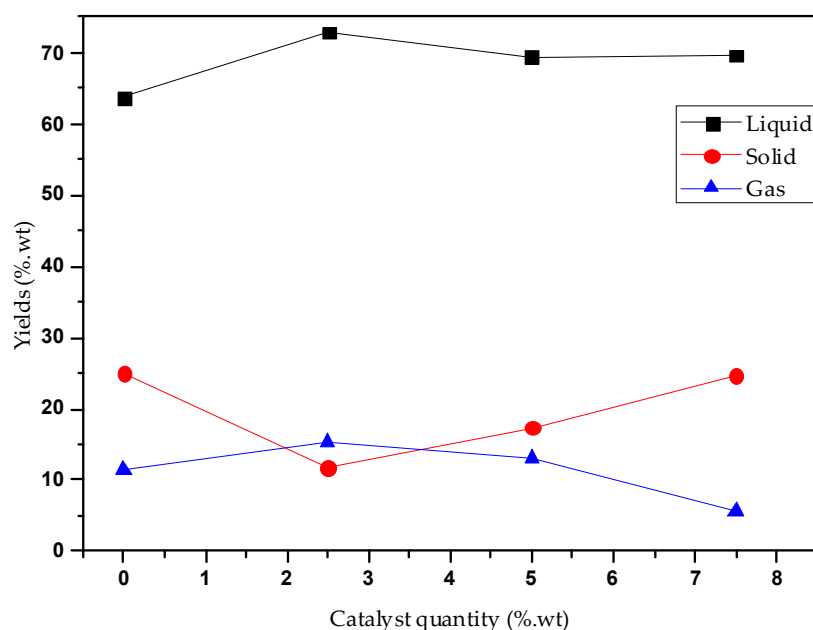


**Figure 15.** Effect of catalyst quantity on the catalytic upgrading of WEEE plastics.

Nunome et al. studied the generation behavior of tar (PAH) during pyrolysis of ABS and concluded that PAHs form due to incorporation of  $C_2$  and  $C_2H_2$  units and that they were formed mostly by nitrogen-containing hetero-PAHs, oxygen-containing hetero-PAHs, and PAH's. They did not use any catalysts but used temperatures greater than  $700\text{ }^\circ\text{C}$  [87]. The same behavior was found for the WEEE plastic bio-oil in this work, but the surface area provided by the catalyst was responsible for the increase in those types of reactions, explaining why there was a reduction of gas yields with increasing bed height. It was observed that there was an increase in char generated, suggesting that the increased bed height may allow some reflux to happen, effectively increasing the residence time of the process as a whole, including affecting the production of char in reactor R-1. Zhang et al. conducted 2-stage pyrolysis of LDPE using activated carbon as a catalyst, and they found that using a catalyst of high surface area and lower micropore structure increases formation of aromatic compounds and PAHs. They reported that chemical activation enlarged pore volume but reduced micropore structure. There were medium gas yields, though (30%), suggesting that smaller products of reaction got through the porous structure of the catalyst, different from ABS. The chain radicals formed by LDPE are indeed much smaller than ABS pyrolysis products, and the gas composition revealed an increased presence of hydrogen. A similar behavior was observed for the higher temperature of the pyrolysis process of LDPE, producing mainly mono-aromatic and double-ring aromatics such as naphthalene [88].

### 3.4.2. Physical–Chemical Characteristics and Chemical Composition of Bio-Oil Obtained through Catalytic Upgrading

The same procedure for calculation of mean values for the physical–chemical properties determined for thermal cracking was used for the catalytic experiments. Mass fractions, measured properties, and mean calculated values of density, viscosity, and acid value of the upgraded bio-oil are shown in Table 7.

**Table 7.** Weighted average of determined physical–chemical properties and their respective measured properties of time fractions for catalytic upgrading experiments.

Catalyst Quantity (%)	Reaction Time (min)	Bio-Oil Quantity (g)	Density (g/cm <sup>3</sup> )	Viscosity (mm <sup>2</sup> /s)	Acid Value (mg KOH/g)
0.0	15	103.2	0.91	1.46	33.0
	30	95.5	0.98	1.36	24.8
	45	94.7	0.96	1.36	77
	60	89.1	0.91	1.32	28.3
	<b>Total</b>	<b>382.5</b>	<b>0.94</b>	<b>1.38</b>	<b>40.8</b>
2.5	30	169.8	0.90	0.93	16.8
	45	138.2	0.92	1.28	18.8
	60	129.7	0.92	1.52	23.0
	<b>Total</b>	<b>437.7</b>	<b>0.91</b>	<b>1.21</b>	<b>19.3</b>
5.0	15	90.4	0.91	1.06	10.4
	30	103.5	0.89	0.94	14.4
	45	104.2	0.92	1.34	21.6
	60	119.1	0.92	1.34	15.7
	<b>Total</b>	<b>417.2</b>	<b>0.91</b>	<b>1.18</b>	<b>15.7</b>
7.5	15	127.7	0.88	0.99	33.8
	30	106.6	0.90	1.19	20.8
	45	73.7	0.90	1.65	15.3
	60	110.4	0.90	1.61	1.15
	<b>Total</b>	<b>418.4</b>	<b>0.89</b>	<b>1.38</b>	<b>16.6</b>

Overall, density reduced slightly, while viscosity tended to increase when compared to the thermal cracking experiments at 450 °C due to formation of PAHs and double-ring nitrogenated aromatics. Acid values were remarkably lower, suffering a reduction of over 50%. Contact with the thermally heated catalyst increased residence time of vapors, allowing it to reach later stages of cracking and, possibly, obtain better deoxygenation of phenolic compounds present. Acid value analysis is not that common in research into pyrolysis fuels, even though fuel acidity is a critical measurement for adequate functioning of a compression–ignition engine. This is mainly because acid value is an analysis tool for vegetable oil and the biodiesel industry and is more closely related to lipid-based feedstocks. When pyrolysis initiates, fatty acids are produced and later converted to hydrocarbons; the acid value gives insight into conversion of pyrolysis of oils and fats [55,56,65]. For plastic feedstocks, only a few studies have published acid value measurements [45] because acid value is related to the presence of oxygenated compounds and most plastic feedstocks contain minimal amounts of oxygen. For WEEE plastic, though, polycarbonate material is present and can possibly generate phenolic compounds. Wang et al. conducted upgrading of a vinyl-based plastic and found acid values of 17.8 mg KOH/g for the plastic pyrolysis oil and acid values lower than 6 mg KOH/g for the upgraded bio-oil, indicating better deoxygenation.

In the case of polymers containing flame retardants and PVC, there is a possibility of generating inorganic acids such as HCN, HCl, and even NH<sub>3</sub> that could contribute to the balance of acidity in bio-oil [79,80]. Supposedly, most of these compounds are gases and would be released in the pyrolysis process. They could accumulate in the water phase, but these experiments produced only an organic phase. They could instead react with organic compounds, forming brominated or chlorinated substances different from the

original substances. The chemical composition of both thermal cracking and upgrading experiments showed the presence of brominated compounds but not chlorinated ones. The organobromine compounds detected in the GC/MS were 5-Bromo-2-methoxy-1,3-dimethylbenzene and bromophenol. Commonly-used brominated flame retardants are polybrominated diphenyl ethers and tetrabromobisphenol A, which can also contribute to phenolic compound formation. Table 8 presents the mean composition of brominated compounds in the bio-oil with increasing catalyst quantity, and Figure 16 exemplifies the effect of reaction time on the concentration of brominated compounds for thermal and catalytic experiments. The presence of brominated compounds reduces with reaction time, probably due to initial volatiles of the brominated compounds being produced, and the TG analysis showed early decomposition of the WEEE plastic mix. The composition of brominated compounds increased for the bio-oil produced with the catalyst fixed bed in place, suggesting that the catalyst pore size and volume retained more of the brominated compounds in the liquid bio-oil phase.

**Table 8.** Brominated compound composition of bio-oil obtained through thermal cracking and catalytic upgrading with Si–Al ash pellets at 450 °C.

Catalyst Quantity (%.wt)	Brominated Composition (%.area)
0.0	0.17
2.5	0.59
5.0	0.40
7.5	0.44

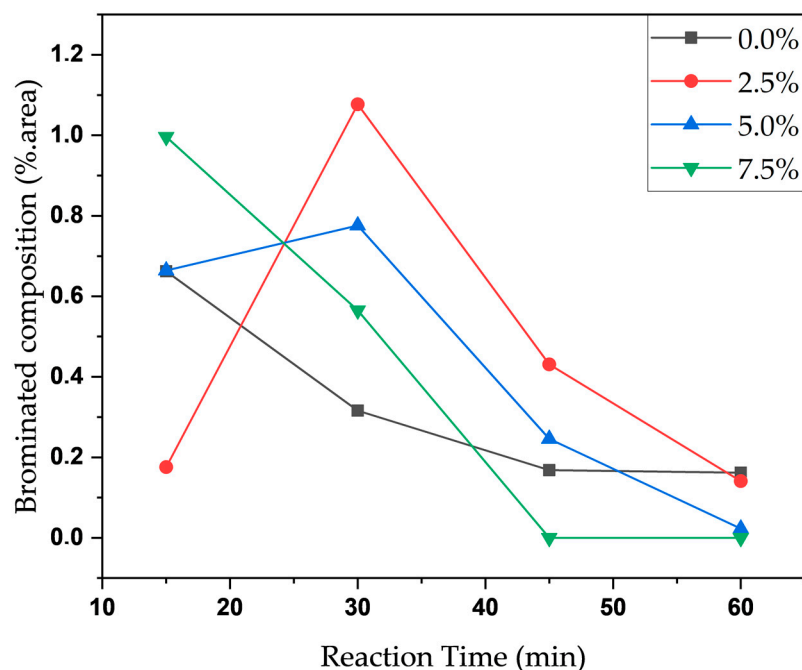


**Figure 16.** Effect of reaction time on brominated compound composition.

Chemical composition revealed an increased presence of PAH in the upgraded bio-oil, indicating the surface area provided by the solid catalyst increased residence time for cracking reactions to occur, allowing secondary product formation by condensation and polymerization reactions. It can be observed that, as the catalyst fixed bed increased in height, the quantity of char formed increased, while gas yields reduced and the liquid phase remained fairly constant. The density and viscosity of bio-oil shown in Table 7 reveal that density tended to decrease while viscosities increased with catalyst quantity for the bio-oil, suggesting that the catalyst with its porous structure allowed the formation of PAH in the

bio-oil and increased char content through aromatization, condensation, and polymerization reactions of the products of reaction [65]. Even though the catalyst is not in contact with the thermal reactor, perhaps some reflux happens between the reactor and catalyst fixed bed, affecting the yields of char obtained. The decreased gas yields indicate that the catalyst could fixate the gas formed into heavier products. A similar trend for the same catalyst was observed in one of our previous works, even though the feedstock was composed of triglyceride materials and high gas yields were obtained. The composition was largely different, though, with linear hydrocarbons comprising the finished product and fatty acids as the principal intermediaries and contaminants; few aromatic products were formed, but PAH was observed as naphthalene in the chemical composition [55]. The bio-oil obtained from WEEE plastic is largely composed of aromatic hydrocarbons such as diphenyl-propane and nitriles such as benzene-butane-nitrile, and this may be why the effect of generating PAHs could be better observed. Additionally, the presence of nitrogenated compounds in the composition of bio-oil introduces the possibility of side reactions of condensation between products of reaction. Indeed, nitrogenated/oxygenated compounds such as quinolines and pyrroles were found in the composition of the nitrogenated fraction.

Figure 17 illustrates the chemical composition change produced with increasing reaction time for all four experiments considering the overall change in the chemical composition. Overall, the chemical composition remained fairly constant throughout all experiments with increasing PAH content and lower oxygenated values. There was little change when comparing the catalytic experiments, though, perhaps because of the little C/F range investigated. Zhang et al. investigated catalytic upgrading of LDPE using an ex situ catalyst fixed bed and a C/F range of 0.6–2.71 to clearly assess the performance of the catalyst used [25]. Fan et al. studied C/F on the catalytic upgrading of LDPE using MgO as the catalyst, and they used a C/F range of 0.06–0.33. Even though there was an effect when comparing thermal and catalytic experiments, the change was remarkably lower for a C/F higher than 0.1 [42]. Nishino et al. also studied C/F and found a fairly constant behavior of chemical composition with a decreasing C/F ratio, but the highest C/F ratio studied was 0.1. They pyrolyzed five different types of plastic on a semi-pilot unit [47].

The same behavior can be observed for all catalytic experiments with respect to changes in chemical composition with reaction time observed for thermal experiments, of almost constant composition. Since the feed is loaded into reactor R-1, pyrolysis vapors arriving at reactor R-2 have the same composition as the vapors comprising thermal cracking bio-oil and gases, so there is no reason to believe that chemical composition would change more effectively with reaction time even when catalytically upgrading the bio-oil. Overall, very little effect of the catalyst is observed when comparing the two set of experiments, and it can be theorized that this is because of rapid deactivation of the catalyst. After runs, the elemental composition of catalyst pellets showed presence of over 40% of carbon as coke, possibly plugging catalyst pores and impeding access of vapors to the catalyst surface. High flowrate and presence of preferential pathways through the catalyst fixed bed could also be responsible for the small catalytic effect of the Si–Al ash pellets. Nevertheless, chemical composition analysis of time samples of bio-oil could be used to effectively check catalyst activity when comparing thermal cracking and catalytic upgrading of WEEE plastics.

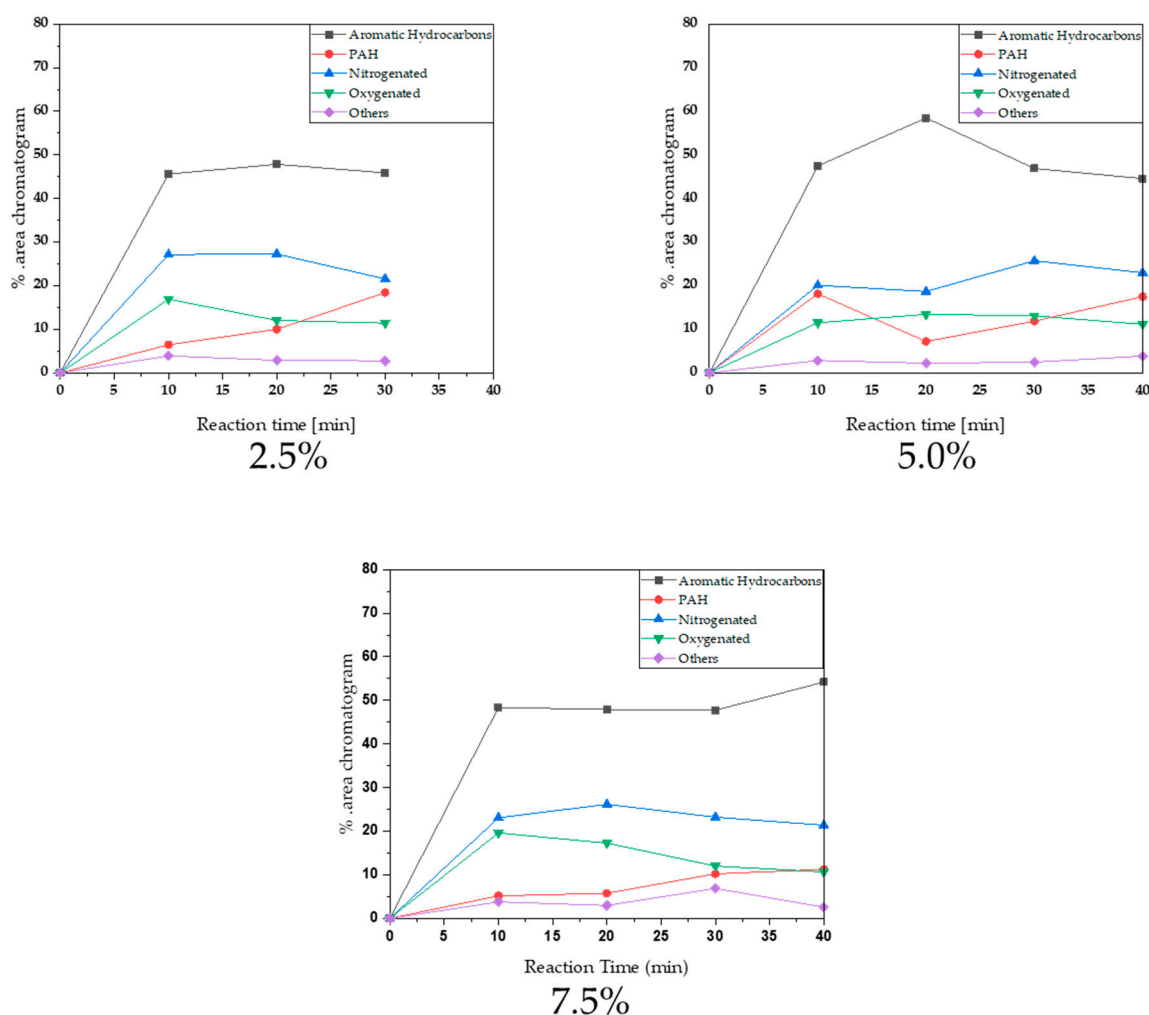


**Figure 17.** Reaction time effect on chemical composition of bio-oil obtained through catalytic upgrading of WEEE plastic at 450 °C, over 2.5, 5.0, and 7.5% catalyst.

#### 4. Conclusions

Computer scraps were pyrolyzed and catalytically upgraded with Si–Al ash pellets as the catalyst to study and investigate the effects of temperature, catalyst quantity, and reaction time on reaction yields, physical–chemical properties, and chemical composition of bio-oil obtained. Catalyst characterization by SEM, EDX, XRD, and XRF revealed a highly porous structure composed of silica and alumina. Feed characterization by TG analysis indicated presence of ABS and PC polymers, as well the possibility of containing brominated compounds such as tetrabromobisphenol as flame retardants. High amounts of gases were produced for low temperatures of cracking, decreasing with an increase in temperature. The opposite trend was observed for the liquid phase. The TG analysis showed a three-peak decomposition of the WEEE plastic mix, indicating that the early decomposition occasioned by the brominated flame-retardant compounds and maintenance of reaction temperature at the low temperature of 350 °C were responsible for the initial high gas yields. Liquid yields increased until 450 °C because of the biggest peak of decomposition at 418 °C. The third decomposition peak and increased char yields may indicate the presence of polycarbonate material for the feed. Acid value analysis showed increased values for higher temperatures, indicating that low temperatures favored deoxygenation reactions and elimination of gases such as HCN and NH<sub>3</sub>. Mostly, the bio-oil is composed of aromatic hydrocarbons such as benzene derivatives (benzene, 1,1'-(1,3-propanediyl)bis- and benzene(1-methylethyl)-); styrene derivatives (styrene and methyl-styrene); nitrogenated compounds derived from nitriles such as benzene–butane–nitrile and other nitrogenated

aromatic compounds; and PAH such as ramified naphthalenes and phenolic compounds (phenol and cumenol). Catalytic upgrading favored production of char and reduced production of gases, affecting density and viscosity of bio-oil produced due to increased presence of PAHs and hetero-atom PAHs (nitrogenated and oxygenated) produced by incorporation of smaller hydrocarbon gases produced. Some reflux of products is suggested from reactor R-2 to R-1, explaining the increase in char content with increased bed height. The acid value reduced to values around 17 mg KOH/g, indicating better deoxygenation than in thermal experiments. Organobromine content tended to decrease with reaction time, but showed higher values for the catalytic upgrading experiments. Overall, the chemical composition of bio-oil obtained (thermal cracking or catalytic upgrading) remained fairly constant with respect to reaction time, even though composition of the feed changes in a semi-batch reactor. This confirms that chemical composition and physical–chemical property analysis with respect to reaction time is a powerful tool of analysis of pyrolysis and catalytic upgrading processes, even when using different types of feedstocks.

**Supplementary Materials:** The following supporting information can be downloaded at: <https://www.mdpi.com/article/10.3390/en16010541/s1>, Table S1: Classes of compounds, summation of peak areas, CAS number, and retention times of chemical compounds identified by GC-MS in bio-oil by thermal cracking of WEEE plastic at 350 °C, 1.0 atm, reaction time = 30 min, in semi-pilot scale two-stage reactor of 2.0 L. Table S2: Classes of compounds, summation of peak areas, CAS number, and retention times of chemical compounds identified by GC-MS in bio-oil by thermal cracking of WEEE plastic at 350 °C, 1.0 atm, reaction time = 45 min, in semi-pilot scale two-stage reactor of 2.0 L. Table S3: Classes of compounds, summation of peak areas, CAS number, and retention times of chemical compounds identified by GC-MS in bio-oil by thermal cracking of WEEE plastic at 350 °C, 1.0 atm, reaction time = 60 min, in semi-pilot scale two-stage reactor of 2.0 L. Table S4: Classes of compounds, summation of peak areas, CAS number, and retention times of chemical compounds identified by GC-MS in bio-oil by thermal cracking of WEEE plastic at 400 °C, 1.0 atm, reaction time = 15 min, in semi-pilot scale two-stage reactor of 2.0 L. Table S5: Classes of compounds, summation of peak areas, CAS number, and retention times of chemical compounds identified by GC-MS in bio-oil by thermal cracking of WEEE plastic at 400 °C, 1.0 atm, reaction time = 30 min, in semi-pilot scale two-stage reactor of 2.0 L. Table S6: Classes of compounds, summation of peak areas, CAS number, and retention times of chemical compounds identified by GC-MS in bio-oil by thermal cracking of WEEE plastic at 400 °C, 1.0 atm, reaction time = 45 min, in semi-pilot scale two-stage reactor of 2.0 L. Table S7: Classes of compounds, summation of peak areas, CAS number, and retention times of chemical compounds identified by GC-MS in bio-oil by thermal cracking of WEEE plastic at 400 °C, 1.0 atm, reaction time = 60 min, in semi-pilot scale two-stage reactor of 2.0 L. Table S8: Classes of compounds, summation of peak areas, CAS number, and retention times of chemical compounds identified by GC-MS in bio-oil by thermal cracking of WEEE plastic at 450 °C, 1.0 atm, reaction time = 15 min, in semi-pilot scale two-stage reactor of 2.0 L. Table S9: Classes of compounds, summation of peak areas, CAS number, and retention times of chemical compounds identified by GC-MS in bio-oil by thermal cracking of WEEE plastic at 450 °C, 1.0 atm, reaction time = 30 min, in semi-pilot scale two-stage reactor of 2.0 L. Table S10: Classes of compounds, summation of peak areas, CAS number, and retention times of chemical compounds identified by GC-MS in bio-oil by thermal cracking of WEEE plastic at 450 °C, 1.0 atm, reaction time = 45 min, in semi-pilot scale two-stage reactor of 2.0 L. Table S11: Classes of compounds, summation of peak areas, CAS number, and retention times of chemical compounds identified by GC-MS in bio-oil by thermal cracking of WEEE plastic at 450 °C, 1.0 atm, reaction time = 60 min, in semi-pilot scale two-stage reactor of 2.0 L. Table S12: Classes of compounds, summation of peak areas, CAS number, and retention times of chemical compounds identified by GC-MS in bio-oil by thermal cracking of WEEE plastic at 500 °C, 1.0 atm, reaction time = 15 min, in semi-pilot scale two-stage reactor of 2.0 L. Table S13: Classes of compounds, summation of peak areas, CAS number, and retention times of chemical compounds identified by GC-MS in bio-oil by thermal cracking of WEEE plastic at 500 °C, 1.0 atm, reaction time = 30 min, in semi-pilot scale two-stage reactor of 2.0 L. Table S14: Classes of compounds, summation of peak areas, CAS number, and retention times of chemical compounds identified by GC-MS in bio-oil by thermal cracking of WEEE plastic at 500 °C, 1.0 atm, reaction time = 45 min, in semi-pilot scale two-stage reactor of 2.0 L. Table S15: Classes of compounds, summation of peak

areas, CAS number, and retention times of chemical compounds identified by GC-MS in bio-oil by thermal cracking of WEEE plastic at 500 °C, 1.0 atm, reaction time = 60 min, in semi-pilot scale two-stage reactor of 2.0 L. Table S16: Classes of compounds, summation of peak areas, CAS number, and retention times of chemical compounds identified by GC-MS in bio-oil by catalytic upgrading of WEEE plastic pyrolysis vapors at 450 °C, 1.0 atm, on a fixed catalyst bed loaded with 2.5 %wt of Si–Al ash pellets, reaction time = 30 min, in semi-pilot scale two-stage reactor of 2.0 L. Table S17: Classes of compounds, summation of peak areas, CAS number, and retention times of chemical compounds identified by GC-MS in bio-oil by catalytic upgrading of WEEE plastic pyrolysis vapors at 450 °C, 1.0 atm, on a fixed catalyst bed loaded with 2.5 %wt of Si–Al ash pellets, reaction time = 45 min, in semi-pilot scale two-stage reactor of 2.0 L. Table S18: Classes of compounds, summation of peak areas, CAS number, and retention times of chemical compounds identified by GC-MS in bio-oil by catalytic upgrading of WEEE plastic pyrolysis vapors at 450 °C, 1.0 atm, on a fixed catalyst bed loaded with 2.5 %wt of Si–Al ash pellets, reaction time = 60 min, in semi-pilot scale two-stage reactor of 2.0 L. Table S19: Classes of compounds, summation of peak areas, CAS number, and retention times of chemical compounds identified by GC-MS in bio-oil by catalytic upgrading of WEEE plastic pyrolysis vapors at 450 °C, 1.0 atm, on a fixed catalyst bed loaded with 5.0 %wt of Si–Al ash pellets, reaction time = 15 min, in semi-pilot scale two-stage reactor of 2.0 L. Table S20: Classes of compounds, summation of peak areas, CAS number, and retention times of chemical compounds identified by GC-MS in bio-oil by catalytic upgrading of WEEE plastic pyrolysis vapors at 450 °C, 1.0 atm, on a fixed catalyst bed loaded with 5.0 %wt of Si–Al ash pellets, reaction time = 30 min, in semi-pilot scale two-stage reactor of 2.0 L. Table S21: Classes of compounds, summation of peak areas, CAS number, and retention times of chemical compounds identified by GC-MS in bio-oil by catalytic upgrading of WEEE plastic pyrolysis vapors at 450 °C, 1.0 atm, on a fixed catalyst bed loaded with 5.0 %wt of Si–Al ash pellets, reaction time = 45 min, in semi-pilot scale two-stage reactor of 2.0 L. Table S22: Classes of compounds, summation of peak areas, CAS number, and retention times of chemical compounds identified by GC-MS in bio-oil by catalytic upgrading of WEEE plastic pyrolysis vapors at 450 °C, 1.0 atm, on a fixed catalyst bed loaded with 5.0 %wt of Si–Al ash pellets, reaction time = 60 min, in semi-pilot scale two-stage reactor of 2.0 L. Table S23: Classes of compounds, summation of peak areas, CAS number, and retention times of chemical compounds identified by GC-MS in bio-oil by catalytic upgrading of WEEE plastic pyrolysis vapors at 450 °C, 1.0 atm, on a fixed catalyst bed loaded with 7.5 %wt of Si–Al ash pellets, reaction time = 15 min, in semi-pilot scale two-stage reactor of 2.0 L. Table S24: Classes of compounds, summation of peak areas, CAS number, and retention times of chemical compounds identified by GC-MS in bio-oil by catalytic upgrading of WEEE plastic pyrolysis vapors at 450 °C, 1.0 atm, on a fixed catalyst bed loaded with 7.5 %wt of Si–Al ash pellets, reaction time = 30 min, in semi-pilot scale two-stage reactor of 2.0 L. Table S25: Classes of compounds, summation of peak areas, CAS number, and retention times of chemical compounds identified by GC-MS in bio-oil by catalytic upgrading of WEEE plastic pyrolysis vapors at 450 °C, 1.0 atm, on a fixed catalyst bed loaded with 7.5 %wt of Si–Al ash pellets, reaction time = 45 min, in semi-pilot scale two-stage reactor of 2.0 L. Table S26: Classes of compounds, summation of peak areas, CAS number, and retention times of chemical compounds identified by GC-MS in bio-oil by catalytic upgrading of WEEE plastic pyrolysis vapors at 450 °C, 1.0 atm, on a fixed catalyst bed loaded with 7.5 %wt of Si–Al ash pellets, reaction time = 60 min, in semi-pilot scale two-stage reactor of 2.0 L.

**Author Contributions:** A.F.d.F.C. contributed with formal analysis and writing original draft preparation, investigation and methodology, C.C.F. contributed with investigation and methodology, S.P.A.d.P. contributed with XRF and XRD investigation and methodology, M.C.S. contributed with investigation and methodology, L.G.S.M. contributed with chemical analysis, A.C.G.d.A.d.F. contributed with chemical analysis, N.M.M. contributed with contributed with resources and chemical analysis, F.P.d.C.A. contributed with chemical analysis, R.M.R.C. and C.E.F.d.C. contributed with TG chemical and formal analysis, S.A.P.d.M. and I.W.d.S.B. contributed with investigation, methodology and chemical analysis, D.A.R.d.C. contributed with formal analysis, investigation and methodology, S.D.J. contributed with resources and chemical analysis, L.E.P.B. with co-supervision and resources, and N.T.M. and L.P.B. contributed with supervision, conceptualization, and data curation. All authors have read and agreed to the published version of the manuscript.

**Funding:** This research received no external funding.

**Acknowledgments:** N.T.M. would like to acknowledge and dedicate this research in memory to Hélio da Silva Almeida. He used to work at the Faculty of Sanitary and Environmental Engineering/UFPa and passed away on 13 March 2021. His contagious joy, dedication, intelligence, honesty, seriousness, and kindness will always be remembered in our hearts.

**Conflicts of Interest:** The authors declare no conflict of interest.

### Abbreviations

ABS	Acrylonitrile–butadiene–styrene copolymer
Br–ABS	Brominated ABS
C/F	Catalyst-to-feed ratio
EDX	Dispersive energy spectrometry
GC/MS	Gas chromatography/mass spectrometry
HDPE	High density polyethylene
HIPS	High impact polystyrene
LDPE	Low density polyethylene
MHSW	Municipal household solid waste
NCG	Non-condensable gas
PAH	Polycyclic aromatic hydrocarbon
PC	Polycarbonate
PE	Polyethylene
PET	Polyethylene terephthalate
PP	Polypropylene
PVC	Polyvinylchloride
SEM	Scanning electron microscopy
TG	Thermogravimetry
XRD	X-ray diffraction
XRF	X-ray fluorescence
WEEE	Waste electric and electronic equipment

### References

1. Thiounn, T.; Smith, R.C. Advances and Approaches for Chemical Recycling of Plastic Waste. *J. Polym. Sci.* **2020**, *58*, 1347–1364. [[CrossRef](#)]
2. Kasar, P.; Sharma, D.K.; Ahmaruzzaman, M. Thermal and Catalytic Decomposition of Waste Plastics and Its Co-Processing with Petroleum Residue through Pyrolysis Process. *J. Clean. Prod.* **2020**, *265*, 121639. [[CrossRef](#)]
3. *Global Plastics Outlook*; OECD: Paris, France, 2022; ISBN 9789264654945.
4. Neuwahl, F.; Cusano, G.; Benavides, J.G.; Holbrook, S.; Roudier, S. *Best Available Techniques (BAT) Reference Document for Waste Incineration*; European Commission, Publications Office of the European Union: Luxembourg, 2019; ISSN 1831-9424. [[CrossRef](#)]
5. Wong, S.L.; Ngadi, N.; Abdullah, T.A.T.; Inuwa, I.M. Current State and Future Prospects of Plastic Waste as Source of Fuel: A Review. *Renew. Sustain. Energy Rev.* **2015**, *50*, 1167–1180. [[CrossRef](#)]
6. Papari, S.; Bamdad, H.; Berruti, F. Pyrolytic Conversion of Plastic Waste to Value-Added Products and Fuels: A Review. *Materials* **2021**, *14*, 2586. [[CrossRef](#)]
7. Jha, K.K.; Kannan, T.T.M. Recycling of Plastic Waste into Fuel by Pyrolysis—A Review. *Mater. Today Proc.* **2021**, *37*, 3718–3720. [[CrossRef](#)]
8. Panda, A.K.; Singh, R.K.; Mishra, D.K. Thermolysis of Waste Plastics to Liquid Fuel: A Suitable Method for Plastic Waste Management and Manufacture of Value Added Products—A World Prospective. *Renew. Sustain. Energy Rev.* **2010**, *14*, 233–248. [[CrossRef](#)]
9. Jahirul, M.I.; Rasul, M.G.; Schaller, D.; Khan, M.M.K.; Hasan, M.M.; Hazrat, M.A. Transport Fuel from Waste Plastics Pyrolysis—A Review on Technologies, Challenges and Opportunities. *Energy Convers. Manag.* **2022**, *258*, 115451. [[CrossRef](#)]
10. Williams, P.T.; Slaney, E. Analysis of Products from the Pyrolysis and Liquefaction of Single Plastics and Waste Plastic Mixtures. *Resour. Conserv. Recycl.* **2007**, *51*, 754–769. [[CrossRef](#)]
11. Mangesh, V.L.; Padmanabhan, S.; Tamizhdurai, P.; Ramesh, A. Experimental Investigation to Identify the Type of Waste Plastic Pyrolysis Oil Suitable for Conversion to Diesel Engine Fuel. *J. Clean. Prod.* **2020**, *246*, 119066. [[CrossRef](#)]
12. Sharma, B.K.; Moser, B.R.; Vermillion, K.E.; Doll, K.M.; Rajagopalan, N. Production, Characterization and Fuel Properties of Alternative Diesel Fuel from Pyrolysis of Waste Plastic Grocery Bags. *Fuel Process. Technol.* **2014**, *122*, 79–90. [[CrossRef](#)]
13. Li, D.; Lei, S.; Wang, P.; Zhong, L.; Ma, W.; Chen, G. Study on the Pyrolysis Behaviors of Mixed Waste Plastics. *Renew. Energy* **2021**, *173*, 662–674. [[CrossRef](#)]

14. Muhammad, C.; Onwudili, J.A.; Williams, P.T. Catalytic Pyrolysis of Waste Plastic from Electrical and Electronic Equipment. *J. Anal. Appl. Pyrolysis* **2015**, *113*, 332–339. [[CrossRef](#)]
15. Sudhir, M.; Desai, B.; Chetan, M.; Galage, K. Production and Analysis of Pyrolysis Oil from Waste Plastic in Kolhapur City. *Int. J. Eng. Res. Gen. Sci.* **2015**, *3*, 590–595.
16. Lee, K.H.; Shin, D.H. Characteristics of Liquid Product from the Pyrolysis of Waste Plastic Mixture at Low and High Temperatures: Influence of Lapse Time of Reaction. *Waste Manag.* **2007**, *27*, 168–176. [[CrossRef](#)] [[PubMed](#)]
17. Kiran, N.; Ekinici, E.; Snape, C.E. Recycling of Plastic Wastes via Pyrolysis. *Resour. Conserv. Recycl.* **2000**, *29*, 273–283. [[CrossRef](#)]
18. Sogancioglu, M.; Ahmetli, G.; Yel, E. A Comparative Study on Waste Plastics Pyrolysis Liquid Products Quantity and Energy Recovery Potential. *Energy Procedia* **2017**, *118*, 221–226. [[CrossRef](#)]
19. Kumar, S.; Prakash, R.; Murugan, S.; Singh, R.K. Performance and Emission Analysis of Blends of Waste Plastic Oil Obtained by Catalytic Pyrolysis of Waste HDPE with Diesel in a CI Engine. *Energy Convers. Manag.* **2013**, *74*, 323–331. [[CrossRef](#)]
20. Miskolczi, N.; Nagy, R. Hydrocarbons Obtained by Waste Plastic Pyrolysis: Comparative Analysis of Decomposition Described by Different Kinetic Models. *Fuel Process. Technol.* **2012**, *104*, 96–104. [[CrossRef](#)]
21. Miskolczi, N.; Angyal, A.; Bartha, L.; Valkai, I. Fuels by Pyrolysis of Waste Plastics from Agricultural and Packaging Sectors in a Pilot Scale Reactor. *Fuel Process. Technol.* **2009**, *90*, 1032–1040. [[CrossRef](#)]
22. Papuga, S.V.; Gvero, P.M.; Vukić, L.M. Temperature and Time Influence on the Waste Plastics Pyrolysis in the Fixed Bed Reactor. *Therm. Sci.* **2016**, *20*, 731–741. [[CrossRef](#)]
23. Khan, M.Z.H.; Sultana, M.; Al-Mamun, M.R.; Hasan, M.R. Pyrolytic Waste Plastic Oil and Its Diesel Blend: Fuel Characterization. *J. Env. Public Health* **2016**, *2016*, 1–6. [[CrossRef](#)] [[PubMed](#)]
24. Das, P.; Tiwari, P. The Effect of Slow Pyrolysis on the Conversion of Packaging Waste Plastics (PE and PP) into Fuel. *Waste Manag.* **2018**, *79*, 615–624. [[CrossRef](#)] [[PubMed](#)]
25. Zhang, Y.; Duan, D.; Lei, H.; Villota, E.; Ruan, R. Jet Fuel Production from Waste Plastics via Catalytic Pyrolysis with Activated Carbons. *Appl. Energy* **2019**, *251*, 113337. [[CrossRef](#)]
26. Ratnasari, D.K.; Nahil, M.A.; Williams, P.T. Catalytic Pyrolysis of Waste Plastics Using Staged Catalysis for Production of Gasoline Range Hydrocarbon Oils. *J. Anal. Appl. Pyrolysis* **2017**, *124*, 631–637. [[CrossRef](#)]
27. Xue, Y.; Johnston, P.; Bai, X. Effect of Catalyst Contact Mode and Gas Atmosphere during Catalytic Pyrolysis of Waste Plastics. *Energy Convers. Manag.* **2017**, *142*, 441–451. [[CrossRef](#)]
28. Singh, R.K.; Ruj, B.; Sadhukhan, A.K.; Gupta, P.; Tigga, V.P. Waste Plastic to Pyrolytic Oil and Its Utilization in CI Engine: Performance Analysis and Combustion Characteristics. *Fuel* **2020**, *262*, 116539. [[CrossRef](#)]
29. Kremer, I.; Tomić, T.; Katančić, Z.; Erceg, M.; Papuga, S.; Vuković, J.P.; Schneider, D.R. Catalytic Pyrolysis of Mechanically Non-Recyclable Waste Plastics Mixture: Kinetics and Pyrolysis in Laboratory-Scale Reactor. *J. Env. Manag.* **2021**, *296*, 113145. [[CrossRef](#)] [[PubMed](#)]
30. Barbarias, I.; Lopez, G.; Artetxe, M.; Arregi, A.; Bilbao, J.; Olazar, M. Valorisation of Different Waste Plastics by Pyrolysis and In-Line Catalytic Steam Reforming for Hydrogen Production. *Energy Convers. Manag.* **2018**, *156*, 575–584. [[CrossRef](#)]
31. Huo, E.; Lei, H.; Liu, C.; Zhang, Y.; Xin, L.; Zhao, Y.; Qian, M.; Zhang, Q.; Lin, X.; Wang, C.; et al. Jet Fuel and Hydrogen Produced from Waste Plastics Catalytic Pyrolysis with Activated Carbon and MgO. *Sci. Total Environ.* **2020**, *727*, 138411. [[CrossRef](#)] [[PubMed](#)]
32. Pratt, L.M.; Kim, J.; Lo, H.Y.; Xiao, D. Brown Grease Pyrolysis under Pressure: Extending the Range of Reaction Conditions and Hydrocarbon Product Distributions. *Fuel* **2021**, *289*, 119782. [[CrossRef](#)]
33. Balcazar, J.G.C.; Dias, R.A.; Balestieri, J.A.P. Analysis of Hybrid Waste-to-Energy for Medium-Sized Cities. *Energy* **2013**, *55*, 728–741. [[CrossRef](#)]
34. Hasan, M.M.; Rasul, M.G.; Khan, M.M.K.; Ashwath, N.; Jahirul, M.I. Energy Recovery from Municipal Solid Waste Using Pyrolysis Technology: A Review on Current Status and Developments. *Renew. Sustain. Energy Rev.* **2021**, *145*, 111073. [[CrossRef](#)]
35. Sikarwar, V.S.; Zhao, M.; Clough, P.; Yao, J.; Zhong, X.; Memon, M.Z.; Shah, N.; Anthony, E.J.; Fennell, P.S. An Overview of Advances in Biomass Gasification. *Energy Environ. Sci.* **2016**, *9*, 2939–2977. [[CrossRef](#)]
36. Sikarwar, V.S.; Zhao, M.; Fennell, P.S.; Shah, N.; Anthony, E.J. Progress in Biofuel Production from Gasification. *Prog. Energy Combust. Sci.* **2017**, *61*, 189–248. [[CrossRef](#)]
37. Buekens, A.; Yang, J. Recycling of WEEE Plastics: A Review. *J. Mater. Cycles Waste Manag.* **2014**, *16*, 415–434. [[CrossRef](#)]
38. Hall, W.J.; Williams, P.T. Removal of Organobromine Compounds from the Pyrolysis Oils of Flame Retarded Plastics Using Zeolite Catalysts. *J. Anal. Appl. Pyrolysis* **2008**, *81*, 139–147. [[CrossRef](#)]
39. Hall, W.J.; Williams, P.T. Analysis of Products from the Pyrolysis of Plastics Recovered from the Commercial Scale Recycling of Waste Electrical and Electronic Equipment. *J. Anal. Appl. Pyrolysis* **2007**, *79*, 375–386. [[CrossRef](#)]
40. Hall, W.J.; Williams, P.T. Fast Pyrolysis of Halogenated Plastics Recovered from Waste Computers. *Energy Fuels* **2006**, *20*, 1536–1549. [[CrossRef](#)]
41. Nakaji, Y.; Tamura, M.; Miyaoka, S.; Kumagai, S.; Tanji, M.; Nakagawa, Y.; Yoshioka, T.; Tomishige, K. Low-Temperature Catalytic Upgrading of Waste Polyolefinic Plastics into Liquid Fuels and Waxes. *Appl. Catal. B* **2021**, *285*, 119805. [[CrossRef](#)]
42. Fan, L.; Zhang, Y.; Liu, S.; Zhou, N.; Chen, P.; Liu, Y.; Wang, Y.; Peng, P.; Cheng, Y.; Addy, M.; et al. Ex-Situ Catalytic Upgrading of Vapors from Microwave-Assisted Pyrolysis of Low-Density Polyethylene with MgO. *Energy Convers. Manag.* **2017**, *149*, 432–441. [[CrossRef](#)]

43. Fan, L.; Su, Z.; Wu, J.; Xiao, Z.; Huang, P.; Liu, L.; Jiang, H.; Zhou, W.; Liu, S.; Ruan, R. Integrating Continuous-Stirred Microwave Pyrolysis with Ex-Situ Catalytic Upgrading for Linear Low-Density Polyethylene Conversion: Effects of Parameter Conditions. *J. Anal. Appl. Pyrolysis* **2021**, *157*, 105213. [[CrossRef](#)]
44. Ma, C.; Yu, J.; Yan, Q.; Song, Z.; Wang, K.; Wang, B.; Sun, L. Pyrolysis-Catalytic Upgrading of Brominated High Impact Polystyrene over Fe and Ni Modified Catalysts: Influence of HZSM-5 and MCM-41 Catalysts. *Polym. Degrad. Stab.* **2017**, *146*, 1–12. [[CrossRef](#)]
45. Wang, S.; Kim, H.; Lee, D.; Lee, Y.R.; Won, Y.; Hwang, B.W.; Nam, H.; Ryu, H.J.; Lee, K.H. Drop-in Fuel Production with Plastic Waste Pyrolysis Oil over Catalytic Separation. *Fuel* **2021**, *305*, 121440. [[CrossRef](#)]
46. Bagri, R.; Williams, P.T. Catalytic Pyrolysis of Polyethylene. *J. Anal. Appl. Pyrolysis* **2002**, *63*, 29–41. [[CrossRef](#)]
47. Nishino, J.; Itoh, M.; Ishinomori, T.; Kubota, N.; Uemichi, Y. Development of a Catalytic Cracking Process for Converting Waste Plastics to Petrochemicals. *J. Mater. Cycles Waste Manag.* **2003**, *5*, 89–93. [[CrossRef](#)]
48. Dai, L.; Zhou, N.; Cobb, K.; Chen, P.; Wang, Y.; Liu, Y.; Zou, R.; Lei, H.; Mohamed, B.A.; Cheng, Y.; et al. Insights into Structure–Performance Relationship in the Catalytic Cracking of High Density Polyethylene. *Appl. Catal. B* **2022**, *318*, 121835. [[CrossRef](#)]
49. Zhou, N.; Dai, L.; Lyu, Y.; Wang, Y.; Li, H.; Cobb, K.; Chen, P.; Lei, H.; Ruan, R. A Structured Catalyst of ZSM-5/SiC Foam for Chemical Recycling of Waste Plastics via Catalytic Pyrolysis. *Chem. Eng. J.* **2022**, *440*, 135836. [[CrossRef](#)]
50. Hwang, K.R.; Choi, S.A.; Choi, I.H.; Lee, K.H. Catalytic Cracking of Chlorinated Heavy Wax from Pyrolysis of Plastic Wastes to Low Carbon-Range Fuels: Catalyst Effect on Properties of Liquid Products and Dechlorination. *J. Anal. Appl. Pyrolysis* **2021**, *155*, 105090. [[CrossRef](#)]
51. Marino, A.; Aloise, A.; Hernando, H.; Feroso, J.; Cozza, D.; Giglio, E.; Migliori, M.; Pizarro, P.; Giordano, G.; Serrano, D.P. ZSM-5 Zeolites Performance Assessment in Catalytic Pyrolysis of PVC-Containing Real WEEE Plastic Wastes. *Catal. Today* **2022**, *390–391*, 210–220. [[CrossRef](#)]
52. Ma, C.; Yu, J.; Chen, T.; Yan, Q.; Song, Z.; Wang, B.; Sun, L. Influence of Fe Based ZSM-5 Catalysts on the Vapor Intermediates from the Pyrolysis of Brominated Acrylonitrile-Butadiene-Styrene Copolymer (Br-ABS). *Fuel* **2018**, *230*, 390–396. [[CrossRef](#)]
53. Shafaghat, H.; Gulshan, S.; Johansson, A.C.; Evangelopoulos, P.; Yang, W. Selective Recycling of BTX Hydrocarbons from Electronic Plastic Wastes Using Catalytic Fast Pyrolysis. *Appl. Surf. Sci.* **2022**, *605*, 125964. [[CrossRef](#)]
54. Chen, T.; Yu, J.; Ma, C.; Bikane, K.; Sun, L. Catalytic Performance and Debromination of Fe–Ni Bimetallic MCM-41 Catalyst for the Two-Stage Pyrolysis of Waste Computer Casing Plastic. *Chemosphere* **2020**, *248*, 125964. [[CrossRef](#)] [[PubMed](#)]
55. Pinto Bernar, L.; Campos Ferreira, C.; Fernando de Freitas Costa, A.; Jorge da Silva Ribeiro, H.; Gomes dos Santos, W.; Martins Pereira, L.; Mathias Pereira, A.; Lobato Moraes, N.; Paula da Costa Assunção, F.; Alex Pereira da Mota, S.; et al. Catalytic Upgrading of Residual Fat Pyrolysis Vapors over Activated Carbon Pellets into Hydrocarbons-like Fuels in a Two-Stage Reactor: Analysis of Hydrocarbons Composition and Physical–Chemistry Properties. *Energies* **2022**, *15*, 4587. [[CrossRef](#)]
56. Ferreira, C.C.; Bernar, L.P.; de Freitas Costa, A.F.; da Silva Ribeiro, H.J.; Santos, M.C.; Moraes, N.L.; Costa, Y.S.; Baia, A.C.F.; Mendonça, N.M.; da Mota, S.A.P.; et al. Improving Fuel Properties and Hydrocarbon Content from Residual Fat Pyrolysis Vapors over Activated Red Mud Pellets in Two-Stage Reactor: Optimization of Reaction Time and Catalyst Content. *Energy* **2022**, *15*, 5595. [[CrossRef](#)]
57. Tseng, R.L. Mesopore Control of High Surface Area NaOH-Activated Carbon. *J. Colloid Interface Sci* **2006**, *303*, 494–502. [[CrossRef](#)]
58. Rocha de Castro, D.; da Silva Ribeiro, H.; Hamoy Guerreiro, L.; Pinto Bernar, L.; Jonatan Bremer, S.; Costa Santo, M.; da Silva Almeida, H.; Duvoisin, S.; Pizarro Borges, L.; Teixeira Machado, N. Production of Fuel-Like Fractions by Fractional Distillation of Bio-Oil from Açai (*Euterpe Oleracea* Mart.) Seeds Pyrolysis. *Energy* **2021**, *14*, 3713. [[CrossRef](#)]
59. Appleby, W.G.; Gibson, J.W.; Good, G.M. Coke Formation in Catalytic Cracking. *Ind. Eng. Chem. Process Des. Dev.* **1962**, *1*, 102–110. [[CrossRef](#)]
60. Fertani-Gmati, M.; Brahim, K.; Khattech, I.; Jemal, M. Thermochemistry and Kinetics of Silica Dissolution in NaOH Solutions: Effect of the Alkali Concentration. *Acta* **2014**, *594*, 58–67. [[CrossRef](#)]
61. David Jackson, S. Processes Occurring during Deactivation and Regeneration of Metal and Metal Oxide Catalysts. *Chem. Eng. J.* **2006**, *120*, 119–125. [[CrossRef](#)]
62. Argyle, M.; Bartholomew, C. Heterogeneous Catalyst Deactivation and Regeneration: A Review. *Catalysts* **2015**, *5*, 145–269. [[CrossRef](#)]
63. Zhang, X.; Sun, L.; Chen, L.; Xie, X.; Zhao, B.; Si, H.; Meng, G. Comparison of Catalytic Upgrading of Biomass Fast Pyrolysis Vapors over CaO and Fe(III)/CaO Catalysts. *J. Anal. Appl. Pyrolysis* **2014**, *108*, 35–40. [[CrossRef](#)]
64. Sun, Z.; Xu, B.; Rony, A.H.; Toan, S.; Chen, S.; Gasem, K.A.M.; Adidharma, H.; Fan, M.; Xiang, W. Thermogravimetric and Kinetics Investigation of Pine Wood Pyrolysis Catalyzed with Alkali-Treated CaO/ZSM-5. *Energy Convers. Manag.* **2017**, *146*, 182–194. [[CrossRef](#)]
65. Chang, C.-C.; Wan, S.-W. China’s Motor Fuels from Tung Oil. *Ind. Eng. Chem.* **1947**, *39*, 1543–1548. [[CrossRef](#)]
66. Vasile, C.; Brebu, M.A.; Karayildirim, T.; Yanik, J.; Darie, H. Feedstock Recycling from Plastic and Thermoset Fractions of Used Computers (I): Pyrolysis. *J. Mater. Cycles Waste Manag.* **2006**, *8*, 99–108. [[CrossRef](#)]
67. Saraji-Bozorgzad, M.; Geissler, R.; Streibel, T.; Mühlberger, F.; Sklorz, M.; Kaisersberger, E.; Denner, T.; Zimmermann, R. Thermogravimetry Coupled to Single Photon Ionization Quadrupole Mass Spectrometry: A Tool To Investigate the Chemical Signature of Thermal Decomposition of Polymeric Materials. *Anal. Chem.* **2008**, *80*, 3393–3403. [[CrossRef](#)]

68. Roussi, A.T.; Vouvoudi, E.C.; Achilias, D.S. Pyrolytic Degradation Kinetics of HIPS, ABS, PC and Their Blends with PP and PVC. *Acta* **2020**, *690*, 178705. [[CrossRef](#)]
69. Jung, S.-H.; Kim, S.-J.; Kim, J.-S. Thermal Degradation of Acrylonitrile–Butadiene–Styrene (ABS) Containing Flame Retardants Using a Fluidized Bed Reactor: The Effects of Ca-Based Additives on Halogen Removal. *Fuel Process. Technol.* **2012**, *96*, 265–270. [[CrossRef](#)]
70. Jung, S.-H.; Kim, S.-J.; Kim, J.-S. The Influence of Reaction Parameters on Characteristics of Pyrolysis Oils from Waste High Impact Polystyrene and Acrylonitrile–Butadiene–Styrene Using a Fluidized Bed Reactor. *Fuel Process. Technol.* **2013**, *116*, 123–129. [[CrossRef](#)]
71. Bhaskar, T.; Murai, K.; Matsui, T.; Brebu, M.A.; Uddin, M.A.; Muto, A.; Sakata, Y.; Murata, K. Studies on Thermal Degradation of Acrylonitrile–Butadiene–Styrene Copolymer (ABS-Br) Containing Brominated Flame Retardant. *J. Anal. Appl. Pyrolysis* **2003**, *70*, 369–381. [[CrossRef](#)]
72. Bridgwater, A.V. Renewable Fuels and Chemicals by Thermal Processing of Biomass. *Chem. Eng. J.* **2003**, *91*, 87–102. [[CrossRef](#)]
73. Mastral, F.J.; Esperanza, E.; García, P.; Juste, M. Pyrolysis of High-Density Polyethylene in a Fluidised Bed Reactor. Influence of the Temperature and Residence Time. *J. Anal. Appl. Pyrolysis* **2002**, *63*, 1–15. [[CrossRef](#)]
74. Al-Salem, S.M.; Lettieri, P. Kinetic Study of High Density Polyethylene (HDPE) Pyrolysis. *Chem. Eng. Res. Des.* **2010**, *88*, 1599–1606. [[CrossRef](#)]
75. Abbas-Abadi, M.S.; Haghighi, M.N.; Yeganeh, H.; McDonald, A.G. Evaluation of Pyrolysis Process Parameters on Polypropylene Degradation Products. *J. Anal. Appl. Pyrolysis* **2014**, *109*, 272–277. [[CrossRef](#)]
76. López, A.; de Marco, I.; Caballero, B.M.; Laresgoiti, M.F.; Adrados, A. Influence of Time and Temperature on Pyrolysis of Plastic Wastes in a Semi-Batch Reactor. *Chem. Eng. J.* **2011**, *173*, 62–71. [[CrossRef](#)]
77. Onwudili, J.A.; Insura, N.; Williams, P.T. Composition of Products from the Pyrolysis of Polyethylene and Polystyrene in a Closed Batch Reactor: Effects of Temperature and Residence Time. *J. Anal. Appl. Pyrolysis* **2009**, *86*, 293–303. [[CrossRef](#)]
78. Maniscalco, M.; la Paglia, F.; Iannotta, P.; Caputo, G.; Scargiali, F.; Grisafi, F.; Brucato, A. Slow Pyrolysis of an LDPE/PP Mixture: Kinetics and Process Performance. *J. Energy Inst.* **2021**, *96*, 234–241. [[CrossRef](#)]
79. Miskolczi, N.; Hall, W.J.; Angyal, A.; Bartha, L.; Williams, P.T. Production of Oil with Low Organobromine Content from the Pyrolysis of Flame Retarded HIPS and ABS Plastics. *J. Anal. Appl. Pyrolysis* **2008**, *83*, 115–123. [[CrossRef](#)]
80. Brebu, M.; Azhar Uddin, M.; Muto, A.; Sakata, Y.; Vasile, C. The Role of Temperature Program and Catalytic System on the Quality of Acrylonitrile-Butadiene-Styrene Degradation Oil. *J. Anal. Appl. Pyrolysis* **2002**, *63*, 43–57. [[CrossRef](#)]
81. Harussani, M.M.; Sapuan, S.M.; Rashid, U.; Khalina, A.; Ilyas, R.A. Pyrolysis of Polypropylene Plastic Waste into Carbonaceous Char: Priority of Plastic Waste Management amidst COVID-19 Pandemic. *Sci. Total Environ.* **2022**, *803*, 149911. [[CrossRef](#)]
82. Manoj, B.; Kunjomana, A.G. Study of Stacking Structure of Amorphous Carbon by X-ray Diffraction Technique. *Int. J. Electrochem. Sci.* **2012**, *7*, 3127–3134.
83. Iwanek (nee Wilczkowska), E.M.; Kirk, D.W. Application of Slow Pyrolysis to Convert Waste Plastics from a Compost-Reject Stream into Py-Char. *Energy* **2022**, *15*, 3072. [[CrossRef](#)]
84. Joni, I.M.; Nulhakim, L.; Panatarani, C. Characteristics of TiO<sub>2</sub> Particles Prepared by Simple Solution Method Using TiCl<sub>3</sub> Precursor. *J. Phys. Conf. Ser.* **2018**, *1080*, 012042. [[CrossRef](#)]
85. Chin, H.S.; Cheong, K.Y.; Razak, K.A. Review on Oxides of Antimony Nanoparticles: Synthesis, Properties, and Applications. *J. Mater. Sci.* **2010**, *45*, 5993–6008. [[CrossRef](#)]
86. Maafa, I. Pyrolysis of Polystyrene Waste: A Review. *Polymer* **2021**, *13*, 225. [[CrossRef](#)] [[PubMed](#)]
87. Nunome, Y.; Suzuki, T.; Nedjalkov, I.; Ueki, Y.; Yoshiie, R.; Naruse, I. Generation Behavior of Tar from ABS, PC, and PE during Pyrolysis and Steam Gasification by Mass Spectrometry. *J. Mater. Cycles Waste Manag.* **2019**, *21*, 1300–1310. [[CrossRef](#)]
88. Zhang, S.; Zhang, H.; Liu, X.; Zhu, S.; Hu, L.; Zhang, Q. Upgrading of Bio-Oil from Catalytic Pyrolysis of Pretreated Rice Husk over Fe-Modified ZSM-5 Zeolite Catalyst. *Fuel Process. Technol.* **2018**, *175*, 17–25. [[CrossRef](#)]

**Disclaimer/Publisher’s Note:** The statements, opinions and data contained in all publications are solely those of the individual author(s) and contributor(s) and not of MDPI and/or the editor(s). MDPI and/or the editor(s) disclaim responsibility for any injury to people or property resulting from any ideas, methods, instructions or products referred to in the content.